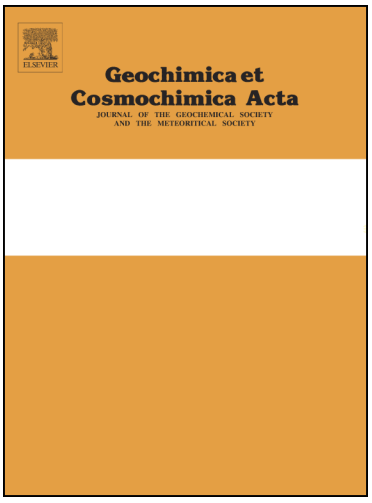

Inverse correlation between the molybdenum and uranium isotope compositions of Upper Devonian black shales caused by changes in local depositional conditions rather than global ocean redox variations

Brian Kendall, Jieying Wang, Wang Zheng, Stephen J. Romaniello, D. Jeffrey Over, Yvonne Bennett, Liyan Xing, Alexandra Kunert, Cameron Boyes, Jian Liu

PII: S0016-7037(20)30038-7
DOI: https://doi.org/10.1016/j.gca.2020.01.026
Reference: GCA 11606

To appear in: *Geochimica et Cosmochimica Acta*

Received Date: 6 August 2019
Revised Date: 9 January 2020
Accepted Date: 10 January 2020

Please cite this article as: Kendall, B., Wang, J., Zheng, W., Romaniello, S.J., Jeffrey Over, D., Bennett, Y., Xing, L., Kunert, A., Boyes, C., Liu, J., Inverse correlation between the molybdenum and uranium isotope compositions of Upper Devonian black shales caused by changes in local depositional conditions rather than global ocean redox variations, *Geochimica et Cosmochimica Acta* (2020), doi: https://doi.org/10.1016/j.gca.2020.01.026

Inverse correlation between the molybdenum and uranium isotope compositions of Upper Devonian black shales caused by changes in local depositional conditions rather than global ocean redox variations

Brian Kendall[1,*], Jieying Wang[1], Wang Zheng[2,3], Stephen J. Romaniello[3,4], D. Jeffrey Over[5], Yvonne Bennett[5], Liyan Xing[1], Alexandra Kunert[1], Cameron Boyes[1], Jian Liu[1]

[1] *Department of Earth and Environmental Sciences, University of Waterloo, 200 University Avenue West, Waterloo, Ontario N2L 3G1, Canada*

[2] *Institute of Surface-Earth System Science, Tianjin University, Tianjin, China*

[3] *School of Earth and Space Exploration, Arizona State University, Tempe, AZ 85287, U.S.A.*

[4] *Department of Earth and Planetary Sciences, University of Tennessee, Knoxville, TN 37996, U.S.A.*

[5] *Department of Geological Sciences, SUNY-Geneseo, Geneseo, NY 14454, U.S.A.*

Revised manuscript submitted to *Geochimica et Cosmochimica Acta*

January 2020

* Correspondence to: bkendall@uwaterloo.ca

Abstract

Coupled Mo-U isotope data from the Upper Devonian Kettle Point Formation (Ontario, Canada) provide a cautionary tale regarding interpretation of global ocean redox conditions using data from euxinic black shales. In the Gore of Chatham core, the Kettle Point black shales have high Mo concentrations (48–473 μg/g) and consistently high Mo/U ratios (≥3 times the Mo/U ratio of modern seawater), suggesting a euxinic depositional environment. These shales yield an inverse correlation ($r = 0.89$, $p < 0.001$) between authigenic U isotope ($\delta^{238}U$ = –0.3‰ to +0.6‰ relative to CRM145 = 0‰) and Mo isotope ($\delta^{98}Mo$ = +0.5‰ to +2.0‰ relative to NIST SRM 3134 = 0.25‰) compositions and a stratigraphic trend upsection towards lower $\delta^{98}Mo$ and higher $\delta^{238}U$. These stratigraphic trends were probably not caused by global ocean redox variation, which should shift both isotope systems in the same direction. Instead, the inverse correlation between the $\delta^{98}Mo$ and $\delta^{238}U$ of the black shales indicates that changes to local depositional conditions in the Chatham Sag affected both isotope systems, consistent with the lithological and elemental evidence for variable paleohydrographic conditions (paleosalinity and sea-level). Black shales with the highest $\delta^{98}Mo$ and lowest $\delta^{238}U$ likely capture the most quantitative removal of Mo and U from more intensely sulfidic bottom waters, and thus most closely approximate global seawater isotope compositions. Lower $\delta^{98}Mo$ and higher $\delta^{238}U$ in the black shales likely record less quantitative Mo and U removal from weakly euxinic bottom waters and thus capture greater sediment-seawater isotope fractionation (lighter Mo isotopes and heavier ^{238}U were preferentially removed from seawater to the sediments). Some samples with low $\delta^{98}Mo$ (0.5-1.0‰) have high V and Mo enrichments, suggesting delivery of V and isotopically light Mo to the sediments by Fe-Mn particulates, but this process does not significantly affect U isotopes (because of weak adsorption of U onto Fe-Mn particulates) and is thus not the major driver of the inverse correlation. The

highest δ^{98}Mo (2.0‰) and lowest δ^{238}U (–0.3‰) from the lower Kettle Point Formation may thus represent minimum and maximum estimates of the Mo and U isotope compositions, respectively, of early Famennian global seawater. The slope of the inverse Mo-U isotope correlation for the Kettle Point black shales broadly parallels data from modern euxinic basins but is shifted to slightly lower isotopic compositions. Hence, Famennian seawater likely had δ^{98}Mo (about 2.0‰ to 2.2‰) and δ^{238}U (about –0.7‰ to –0.4‰) values that were slightly lower than modern global seawater (δ^{98}Mo = 2.3‰; δ^{238}U = –0.4‰), suggesting a mildly greater extent of euxinia (up to 5% of the seafloor) in the Famennian oceans. The opposite stratigraphic trends in δ^{98}Mo and δ^{238}U through the Kettle Point Formation may have caused misinterpretation of global ocean redox conditions if either isotope system was used individually. Hence, paired Mo and U isotope analyses are recommended to determine if stratigraphic trends through euxinic black shales are caused by local depositional changes or global ocean redox variations.

Keywords: Kettle Point Formation; Chatham Sag; Famennian; euxinic; sea-level variation; paleohydrographic conditions

1. INTRODUCTION

The Mo and U isotope compositions of black shales can be used to infer global seawater Mo and U isotope compositions, which in turn provides information about ancient global ocean redox conditions (Barling et al., 2001; Arnold et al., 2004; Weyer et al., 2008; Montoya-Pino et al., 2010). Both Mo and U are redox-sensitive trace metals that have long seawater residence times (~400–500 kyr; Dunk et al., 2002; Miller et al., 2011) in the modern predominantly well-oxygenated oceans, resulting in predominantly homogenous seawater isotopic compositions for

these metals (Barling et al., 2001; Siebert et al., 2003; Stirling et al., 2007; Weyer et al., 2008; Nakagawa et al., 2012; Nägler et al., 2014; Tissot and Dauphas, 2015; Andersen et al., 2016; Noordmann et al., 2016). Burial rates of Mo and U in sediments are at least two orders of magnitude higher in modern euxinic marine environments compared to well-oxygenated settings (see compiled burial rates by Scott et al., 2008; Partin et al., 2013; Reinhard et al., 2013). For each metal, the magnitude of isotope fractionation between sediments and the overlying water column is distinctly different for euxinic environments compared to intermediately reducing (weakly oxygenated and anoxic/non-sulfidic) and oxygenated marine settings. Hence, the global seawater Mo and U isotope compositions are sensitive to the extent of seafloor covered by euxinic waters (Kendall et al., 2009; Dahl et al., 2010, 2011; Tissot and Dauphas, 2015; Andersen et al., 2016; Noordmann et al., 2016; Gilleaudeau et al., 2019). Many studies have exploited the redox-sensitive nature of Mo and U by inferring the seawater isotopic composition of these metals from black shales and carbonates and using this information in isotopic mass-balance models to infer changes in global ocean redox conditions at a variety of timescales (see recent reviews by Kendall et al., 2017 and Andersen et al., 2017).

In practice, using Mo and U isotopes as global paleoredox proxies can be challenging because both local depositional conditions and global ocean redox state influence the isotopic composition of these metals in black shales. Despite continued development in the use of elemental indicators such as sedimentary Fe speciation (Lyons and Severmann, 2006; Poulton and Canfield, 2005, 2011; Raiswell et al., 2018) and Mo/U ratios (Algeo and Tribovillard, 2009) to independently infer local bottom water redox conditions, it is typically not straightforward to infer the magnitude of Mo and U isotope fractionation between organic-rich sediments and the overlying water column. In modern anoxic basins with euxinic bottom waters, near-quantitative removal of

these metals from bottom waters results in preservation of isotopic compositions in sediments that approach global seawater values (Barling et al., 2001; Arnold et al., 2004; Neubert et al., 2008; Noordmann et al., 2015; Bura-Nakić et al., 2018; Brüske et al., in press). However, when non-quantitative removal of Mo and U occurs, the magnitude of local isotope fractionation in euxinic basins depends on a myriad of depositional factors, including bottom water sulfide concentrations (and thus rates of sulfate reduction), degree of basin restriction from the open ocean, basin geometry, and wind/ocean circulation patterns that influence the extent and frequency of water inflow events that partially or fully re-oxygenate deep waters in the basin (Arnold et al., 2004; Neubert et al., 2008; Montoya-Pino et al., 2010; Nägler et al., 2011; Andersen et al., 2014; Holmden et al., 2015; Noordmann et al., 2015; Andersen et al., 2018; Bura-Nakić et al., 2018; Scholz et al., 2018; Brüske et al., in press). These factors can be difficult to constrain precisely for ancient ocean basins, leading to uncertainty in the inferred seawater metal isotope compositions, and thus uncertainty in global ocean redox conditions.

These difficulties can make it challenging to interpret the stratigraphic trends of a single metal isotope system, motivating recent efforts to use paired Mo–U isotope data from the same black shale samples to more robustly infer depositional and redox conditions in ancient oceans (Asael et al., 2013; Kendall at al., 2015; Lu et al., 2017). Recent studies revealed a general inverse correlation between the Mo and U isotope compositions of modern and recent euxinic sediments, including within a single basin (Andersen et al., 2018; Bura-Nakić et al., 2018; Brüske et al., in press). The inverse correlation reflects the opposite directions of Mo and U isotope fractionation during burial of these metals in euxinic sediments. Any expression of mass-dependent Mo isotope fractionation results in preferential removal of lighter Mo isotopes to euxinic sediments (Arnold et al., 2004; Tossell, 2005; Neubert et al., 2008; Dahl et al., 2010), whereas volume-dependent U

isotope fractionation leads to euxinic sediments enriched in heavier ^{238}U compared to lighter ^{235}U (Bigeleisen, 1996; Schauble, 2007; Abe et al., 2008; Weyer et al., 2008). Basins with higher bottom water sulfide concentrations are generally characterized by more efficient removal of Mo and U from bottom waters and hence the sediments from these basins have Mo and U isotope compositions closer to the global seawater isotope composition (Bura-Nakić et al., 2018; Brüske et al., in press). Other depositional processes may also be fingerprinted if both Mo and U isotope data are available for the same samples. Notably, a high flux of Fe-Mn particulates during transient water inflow events into a basin enhances the delivery of isotopically light Mo to euxinic sediments but this process may have relatively little impact on U isotopes because of the weak affinity of U for Fe-Mn (oxyhydr)oxides (Algeo and Tribovillard, 2009; Bura-Nakić et al., 2018; Scholz et al., 2018). In summary, comparison of Mo and U isotope data on the same samples can help distinguish between local depositional versus global redox controls on the Mo and U isotope compositions of black shales.

In this study, we report U and Mo isotope and associated elemental and organic C isotope data from black shales of the largely Famennian Kettle Point Formation (southwestern Ontario, Canada). This case study provides an example of opposing stratigraphic trends and a clear inverse correlation between Mo and U isotope compositions in a predominantly euxinic black shale unit. Drawing from observations of Mo-U isotope systematics in modern euxinic basins, we show that this inverse correlation is most likely the result of a change in local depositional processes rather than global ocean redox conditions. Despite the inverse Mo-U isotope correlation, we show that it is possible to provide some constraints on the global Mo and U isotope composition of Famennian seawater.

2. DEPOSITIONAL ENVIRONMENT OF THE KETTLE POINT FORMATION

The Kettle Point Formation, a potential shale gas resource in southwestern Ontario, is dominated by black shale with subordinate organic-poor green-grey mudstones (Sanford and Brady, 1955; Harris, 1984; Russell, 1985; Armstrong, 1986; Armstrong and Dodge, 2007; Armstrong and Carter, 2010; Hamblin, 2010; Béland-Otis, 2013; Bingham-Koslowski et al., 2016). The Kettle Point Formation is disconformably overlain by the Famennian/Mississippian Bedford Formation of the Port Lambton Group, and disconformably overlies the Givetian Ipperwash Formation or Widder Formation of the Middle Devonian Hamilton Group. The Antrim Shale, Ohio Shale, Chattanooga Shale, and New Albany Shale in the eastern United States overlap stratigraphically with the Kettle Point Formation (Russell, 1985; Hamblin, 2010; Béland-Otis, 2013; Bingham-Koslowski et al., 2016).

The Kettle Point Formation is preserved between the Algonquin and Findlay arches in a structural depression called the Chatham Sag that separates the foreland Appalachian Basin and intracratonic Michigan Basin (Figure 1; Bingham-Koslowski et al., 2016). Deposition of the Kettle Point Formation within this epeiric seaway occurred distal to the Catskill deltaic wedge complex during and following the Acadian Orogeny (Ettensohn, 1985; Hamblin, 2010). The thickest and most complete sections of the Kettle Point Formation (>100 m) occur in the middle of the Chatham Sag (Armstrong and Carter, 2010; Béland-Otis, 2013; Bingham-Koslowski et al., 2016). In these sections, four informal lithostratigraphic units comprise the Kettle Point Formation. Starting at the base of the formation, these units include interbedded green-grey mudstones and black shales containing carbonate concretions (Unit 1), a thick lower black shale interval (Unit 2), interbedded green-grey mudstones and black shales lacking carbonate concretions (Unit 3), and a thick upper

black shale interval (Unit 4) (Bingham-Koslowski et al., 2016). Previous studies have used thin sections and X-ray diffraction (XRD) analysis to determine that the green-grey mudstones and black shales contain quartz and clay minerals (primarily illite but also illite-smectite mixed-layer clays, kaolinite, chlorite, and glauconite) with lesser amounts of dolomite, potassium feldspar, plagioclase feldspar, rutile, calcite, siderite, pyrite, and marcasite (the latter two minerals are found in greater abundance in the black shales; Delitala, 1984; Russell, 1985; Armstrong, 1986; Armstrong and Carter, 2010; Béland-Otis, 2013; Bingham-Koslowski et al., 2016). The Kettle Point Formation predominantly contains Type I and II kerogen from marine sources, and possibly minor Type III kerogen from terrigenous woody plants. Organic matter in the Kettle Point Formation is immature to early mature based on Rock-Eval pyrolysis data and organic petrology (Snowdon, 1984; Obermajer et al., 1997; Beland-Otis, 2013). Hence, post-depositional thermal alteration – a concern for thermally overmature black shales particularly for elemental data (Ardakani et al., 2016; Dickson et al., in press) – should not be significant for the black shales of the Kettle Point Formation.

Significant changes in water depth are thought to have occurred during deposition of the Kettle Point Formation and have been described as two cycles (Units 1-2 and Units 3-4) separated by a significant sea-level fall at the boundary between Units 2 and 3 (Bingham-Koslowski et al., 2016). Sea-level variation likely occurred within Units 1 and 3 as the alternating black shales and green-grey mudstones in these units represent deposition at deeper and shallower water depths, respectively. The black shales from Units 1 and 3 commonly contain laminations rich in silt-sized quartz that may represent higher energy storm or distal turbidite deposits that interrupted periods of quiet-water deposition. Thicker black shale intervals in Units 2 and 4 are thought to have been deposited in consistently deep waters, which is supported by the general absence of silty

laminations in Unit 2 and 4 black shales and lack of grey-green mudstone beds (Bingham-Koslowski et al., 2016). *Callixylon* tree fragments in Units 2 and 4 and possible land plant *Protosalvinia* (*Foerstia)* fossils in Unit 2 suggest inundation of surrounding highlands (Gray and Boucot, 1979; Harris, 1984; Bingham-Koslowski et al., 2016; Quijada et al., 2016).

The lithological variations indicate that water column redox conditions fluctuated during deposition of the Kettle Point Formation. Black shales have high pyrite (up to 16 wt%) and total organic carbon (TOC; up to 15 wt%) contents, low sulfur isotope compositions ($\delta^{34}S$ typically –10‰ to –30‰) and usually lack bioturbation (particularly in Units 2 and 4), suggesting deposition from anoxic bottom waters (Delitala, 1984; Hamblin, 2010; Beland-Otis, 2013; Bingham-Koslowski et al., 2016). Pyrite occurs as finely disseminated crystals and mm- to cm-scale nodules or lenses. The organic-poor green-grey mudstones in Units 1 and 3 contain no body fossils, but are bioturbated (*Chondrites* and *Zoophycos* ichnofossils, which also occur in immediately underlying black shales) and have generally higher $\delta^{34}S$ values that collectively suggest oxic-dysoxic bottom waters (Béland-Otis, 2013; Bingham-Koslowski et al., 2016). Rare red beds also occur within the green-grey mudstones and likely represent the most oxygenated conditions (Bingham-Koslowski et al., 2016). Water column stratification (oxygenated surface waters and anoxic deeper waters) is implied by the presence of *Tasmanites* (algae) and rare fish scale fossils in the black shales (Bingham-Koslowski et al., 2016).

In the Kettle Point Formation, the Frasnian-Famennian boundary was previously placed approximately at the contact between Units 1 and 2 based on conodont data (Winder, 1966; Uyeno et al., 1982) and the occurrence of the Famennian fossil *Protosalvinia* (*Foerstia*) in Unit 2 (Bingham-Koslowski et al., 2016). However, we have made new observations that warrant revision to the placement of the Frasnian-Famennian boundary.

The lowest 2 m of the Kettle Point Formation in the Gore of Chatham core consist of Frasnian strata based on the conodonts *Palmatolepis plana* and *Pa. ljaschenkoae*, indicative of Frasnian zones 9-13 (Klapper, 1989; Klapper and Kirchgasser, 2016). The Frasnian-Famennian boundary is constrained within 50 cm, where the start of Famennian strata are indicated by the occurrence of *Pa. triangularis* at 134.40 m, low in Unit 1. The occurrence of *Pa. prima* and *Pa. lobicornis* higher in Unit 1, characteristic of the *prima* Zone (see Spalletta et al. 2017) or slightly higher, indicate that these strata were deposited in the IIe2 transgressive-regressive (T-R) cycle of Johnson et al. (1985, 1996; see Figure 2 of Over et al., 2019). Winder (1966) reported *Pa. quadrantinodosa quadrantinodosa* and *Pa. marginifera marginifera* from the Sombra 2-6 well that occur low in Unit 2. These observations, and the description of the plant *Protosalvinia (Foerstia)* in the upper part of Unit 2 from numerous wells by Bingham-Koslowski et al. (2016; see Over et al., 2009) indicate the *marginifera* through *granulosus* zones and deposition of Unit 2 during T-R cycle IIe3-4. This suggests that Unit 3 is equivalent to the Chagrin Member and Three Lick interval of the Ohio Shale in the Appalachian Basin, and Unit 4 corresponds to the Cleveland Member of the Ohio Shale and deposition during the major deepening of T-R IIf in the latest Famennian. The rare conodonts reported from the upper Kettle Point Formation by Winder (1966) are long ranging taxa consistent with this interpretation.

3. SAMPLES AND ANALYTICAL METHODS

3.1. Samples

Sixty-five black shale samples of the Kettle Point Formation were collected from the Ontario Geological Survey (OGS) Gore of Chatham core (drilled at 42°37'7.694"N,

82°21'19.599"W) stored at the OGS Oil, Gas, and Salt Resources Library (well T011480) in London, Ontario, Canada. The black shale samples were analyzed for total organic carbon content, total sulfur content, major/minor/trace element abundances, and Mo, U, and organic C isotope compositions. No data are reported in this study for the green-grey mudstones of the Kettle Point Formation.

The Gore of Chatham core contains one of the thickest intervals of the Kettle Point Formation (110.1 m thick; depths: 26.8–136.9 m). In this core, the lithostratigraphy of the Kettle Point Formation is similar to other cores from the middle of the Chatham Sag such that Units 1–4 of Bingham-Koslowski et al. (2016) were easily identified. Specifically, Units 1 and 3 consist of interlaminated black shales interbedded with green-grey mudstone and are located at 120–137 m and 64–91 m, respectively. Units 2 and 4 consist of non-interlaminated black shales and occur at 91–120 m and 27–64 m, respectively. The upper contact of the Kettle Point Formation is not visible in the core. Selected black shale samples for geochemical analysis did not contain macroscopic diagenetic pyrite nodules or carbonate/quartz veins and concretions. Black shales adjacent to the stratigraphically lower contact of green-grey mudstone beds were not sampled because the re-oxygenation events likely associated with green-grey mudstone deposition may have caused penetration of bottom-water O_2 into underlying organic-rich sediments, which can mobilize redox-sensitive elements (resulting in re-deposition of the metals at deeper anoxic sediment depths or loss of the metals to the overlying water column) and thus eradicate depositional geochemical signatures (Crusius and Thomson, 2000).

3.2. Elemental analyses

Major, minor, and trace element concentrations of the Kettle Point black shales were measured in the Metal Isotope Geochemistry Laboratory, Department of Earth and Environmental Sciences, University of Waterloo. All samples were powdered using metal-free methods in an automated agate ball mill. About 100–150 mg of powder was ashed at 550°C overnight to destroy organic matter. In a clean room, the ashed samples were transferred to 22 mL Savillex Teflon beakers and digested using trace-metal grade concentrated acids (2.5 ml HNO_3 plus 0.5 ml HF at 110°C for ≥48 h, 3 ml HCl plus 1 ml HNO_3 at 110°C for ≥48 h, and 2 ml of HCl at 110°C overnight). After digestion, sample solutions were dried and taken up in 5 ml 6M HCl plus a few drops of 0.5% HF. For analysis of elemental concentrations, a weighed portion of the digested sample solution was dried and re-dissolved in 2% HNO_3.

Elemental concentrations were measured on an Agilent 8800 triple quadrupole inductively coupled plasma mass spectrometer (QQQ-ICP-MS). Elements Sc, Ge, In, and Bi were used to correct for instrumental drift during analysis. For each sample, the relative standard deviation (RSD) for the elements of interest (Ca, Mg, Fe, Al, Mo, U, V, Ba, Sr, B, Ga) was nearly always <5% and always <10%. Instrumental accuracy was assessed using the same acid digestion procedure on the United States Geological Survey (USGS) black shale standards SGR-1b (Eocene Green River Shale) and SBC-1 (Pennsylvanian Brush Creek Shale). For these standards, measured concentrations of Ca, Mg, Fe, Mo, U, V, and Sr were within 6% of the certified values, whereas measured Al concentrations were within 11%. Measured Ba concentrations for SBC-1 were within 5% of the certified value (SGR-1b was not used because we observe this standard to yield considerably more variable Ba concentrations than SBC-1). The B and Ga concentrations were measured in separate analytical sessions along with USGS standards SDO-1 (Devonian Ohio

Shale) and T231 (water; for B only) to verify instrumental and procedural accuracy (within 10%). Digestion procedural blanks were negligible (<1%) relative to sample element abundance.

The TOC, total inorganic carbon (TIC), and total sulfur (TS) contents of the samples were measured at the Geoanalytical Laboratory, Department of Earth Sciences, University of Western Ontario. The TOC is calculated as the difference between total carbon determined by combustion in a Leco CS-244 analyzer and TIC determined by acidification. The TS contents were measured by combustion in the CS-244 analyzer. Standards used in this study to verify the accuracy of the carbon and sulfur data included AR-4005, AR-4006, and AR-4007. Deviation of the carbon and sulfur contents of these standards from recommended values was <5% during this study.

3.3. Isotopic analyses

Prior to Mo and U isotope analyses, ion exchange chromatography was carried out in the Metal Isotope Geochemistry Laboratory at Waterloo to obtain purified Mo and U from separate aliquots of the same sample digests. To correct for artificial mass fractionation of Mo and U isotopes caused by ion-exchange chromatography and instrumental analysis, ^{97}Mo–^{100}Mo and ^{233}U–^{236}U (IRMM-3636) double spikes were added to the digested sample solution aliquots before column chromatography. Purification of Mo was accomplished using anion (BioRad AG® 1–X8) followed by cation (BioRad AG® 50W–X8) exchange chromatography (Barling et al., 2001; Arnold et al., 2004) whereas purification of U was done using Eichrom® UTEVA resin (Weyer et al., 2008). The Mo and U isotope analyses were carried out on a Thermo Neptune multi-collector inductively coupled plasma mass spectrometer (MC–ICP–MS) at the W.M. Keck Foundation Laboratory for Environmental Biogeochemistry, School of Earth and Space Exploration, Arizona

State University (ASU). Sample-standard bracketing and an ESI Apex desolvating nebulizer were used for both Mo and U isotope analysis.

Sample U isotope ratios ($\delta^{238}U$) are reported relative to the CRM145 standard as follows:

$$\delta^{238}U\ (‰) = (^{238/235}U_{sample} / {}^{238/235}U_{CRM145} - 1) \times 1000$$

The U isotope standards CRM145, CRM129a, and Ricca were measured repeatedly during this study, yielding average $\delta^{238}U$ values of 0.00 ± 0.07‰ (2SD, n=355), –1.70 ± 0.08‰ (2SD, n=60), and –0.21 ± 0.08‰ (2SD, n=59), respectively. The values for CRM129a and Ricca are statistically identical to the values reported by previous studies (e.g., Weyer et al., 2008; Montoya-Pino et al., 2010; Brennecka et al., 2011a,b; Kendall et al., 2013, 2015; Wang et al., 2015; Chen et al., 2016; Lu et al., 2017; Yang et al., 2017; Zhang et al., 2018). During this study, two measurements of SBC-1 yielded $\delta^{238}U$ values of –0.21‰ and –0.17‰ whereas two measurements of SGR-1b yielded $\delta^{238}U$ values of –0.20‰ and –0.12‰. These values agree well with previously reported average values of –0.24 ± 0.10‰ (2SD, n=3; Yang et al., 2017) and –0.21 ± 0.04‰ (2SD, n=3; Rolison et al., 2017) for SBC-1 and –0.19 ± 0.05‰ (2SD, n=3; Yang et al., 2017) for SGR-1b. Three full powder replicate measurements on samples for this study yielded reproducible $\delta^{238}U$ values within 2SD uncertainties. The assigned 2SD uncertainty of a sample is the 2SD uncertainty of a sample's replicate measurements (typically measured three times) or 0.08‰ (the average long-term uncertainty of CRM129a and Ricca), whichever is greater.

Sample Mo isotope data are reported relative to the NIST SRM 3134 standard as follows (Goldberg et al., 2013; Nägler et al., 2014):

$$\delta^{98}Mo\ (‰) = \{[(^{98/95}Mo)_{sample} / (^{98/95}Mo)_{NIST\text{-}SRM\text{-}3134}) - 1] \times 1000\} + 0.25$$

During this study, the $\delta^{98}Mo$ value for NIST SRM 3134 was 0.33 ± 0.04‰, (2SD, n = 18) relative to the ASU in-house standard RochMo2. In this study, the $\delta^{98}Mo$ of the samples were first

measured relative to RochMo2, and then 0.08‰ was subtracted from the sample δ^{98}Mo to report the data relative to NIST SRM 3134 = 0.25‰. Three full powder replicate measurements on samples for this study yielded reproducible δ^{98}Mo values within 2SD uncertainties. The average δ^{98}Mo for the USGS Devonian black shale standard SDO-1 in this study was 1.07 ± 0.04‰ (2SD, n = 18) relative to NIST SRM 3134 = 0.25‰ and 0.82 ± 0.04‰ (2SD, n = 18) relative to NIST SRM 3134 = 0‰, which is statistically indistinguishable from a previously reported average δ^{98}Mo of 0.82 ± 0.11 ‰ (2SD, n = 145, relative to NIST SRM 3134 = 0‰) for double-spike analyses of SDO-1 on the Thermo Neptune instrument at ASU and the overall averages of 0.80 ± 0.14 ‰ (relative to NIST SRM 3134 = 0‰) and 1.05 ± 0.14 ‰ (relative to NIST SRM 3134 = 0.25‰) for SDO-1 from analyses in four laboratories (Goldberg et al., 2013). The assigned 2SD uncertainty of a sample is the 2SD uncertainty of a sample's replicate measurements (typically measured three times) or 0.11‰ (the average long-term uncertainty of SDO-1), whichever is greater.

Organic carbon isotope measurements were carried out at the Environmental Isotope Laboratory, University of Waterloo. Sample powders were first reacted with dilute HCl to remove carbonate. Subsequently, samples were washed with Nanopure water and dried at 50°C. Samples were combusted at 1750°C using oxygen gas in a Costech Instruments 4010 Elemental Analyser. The carbon isotope composition of the produced CO_2 was analyzed by a Thermo Finnigan Delta Plus XL Continuous Flow Isotope Ratio Mass Spectrometer (CFIRMS). Sample organic carbon isotope data are reported relative to the Vienna Pee Dee Belemnite (VPDB) standard as follows:

$$\delta^{13}C_{org}\ (‰) = [(^{13/12}C)_{sample} / (^{13/12}C)_{VPDB}) - 1] \times 1000$$

Multiple international reference materials (IAEA-CH-3, IAEA-CH-6, USGS-40, USGS-41) and in-house standards (EIL-72, NIST-1577b, NIST-2704) were measured to ensure instrument accuracy. The analytical precision of sample $\delta^{13}C_{org}$ data is 0.2‰ (2SD).

4. RESULTS

Elemental and organic carbon isotope data for the Kettle Point black shales from the Gore of Chatham core are shown in Table 1. The Mo and U isotope data are listed in Table 2.

4.1. Elemental data

The black shales have elevated TOC and TS contents of 3.1–15.6 wt% (mean = 7.9 wt%) and 1.2–6.0 wt% (mean = 2.2 wt%), respectively. The TIC contents are low and range between 0.01 and 1.6 wt% (mean = 0.59 wt%). Hence, the black shales have low carbonate content, consistent with their Ca (0.1–1.5 wt%; mean = 0.38 wt%) and Mg (0.5–1.0 wt%; mean = 0.73 wt%) concentrations. The Fe/Al ratios of the black shales range between 0.35 and 1.0 (mean = 0.47). A wide range of Mo (48–473 μg/g; mean = 123 μg/g), U (9.3–57 μg/g; mean = 25 μg/g), and V (89–1910 μg/g; mean = 555 μg/g) concentrations are observed for the black shales.

To account for the variable detrital and carbonate mineral content of the samples (Tribovillard et al., 2006), authigenic enrichment factors (EF) were calculated for Mo, U, and V using the following equation (average upper crust concentrations used are Mo = 1.1 μg/g, U = 2.7 μg/g, V = 97 μg/g, and Al = 8.15 wt%; Rudnick and Gao, 2003):

$$EF = [metal / Al]_{sample} / [metal / Al]_{average\ upper\ crust}$$

The EF values for Mo, U, and V are 37–463 (mean = 120), 2.9–23 (mean = 10), and 1.5–21 (mean = 6.0), respectively. Metal–TOC correlations (Figure 2) are distinctly better than metal–TS correlations (Figure 3) for Mo and U. Vanadium concentrations are not correlated with TOC or TS contents.

The Sr, Ba, B, and Ga concentrations of the Kettle Point black shales were also measured to enable the use of Sr/Ba and B/Ga ratios as paleosalinity proxies along with TS/TOC ratios. The Sr/Ba, B/Ga, and TS/TOC ratios have ranges of 0.13–1.3 (mean = 0.33), 5.1–9.6 (mean = 6.8), and 0.12–0.66 (mean = 0.30), respectively.

Chemostratigraphic trends of the black shale elemental data do not exhibit a close relationship to the lithostratigraphic units (Units 1-4) of the Kettle Point Formation (Figure 4). Instead, the most striking observation of the redox-sensitive metal data is the maximum enrichments of Mo, V, and U in black shales with high TOC content in upper Unit 4 (above 40 m depth). Lower, but still significant, enrichments of Mo and U occur in Units 1-3 and lower Unit 4. Vanadium enrichments are predominantly low throughout Units 1-3 and increase upsection starting in lower Unit 4. For the paleosalinity proxies, there is a distinctive decrease in the ratios of B/Ga and Sr/Ba ratios upsection but no clear stratigraphic trend for TS/TOC ratios (Figure 5).

4.2. Isotopic data

The bulk $\delta^{98}Mo$ and $\delta^{238}U$ values of the Kettle Point black shales range widely from 0.55‰ to 1.73‰ (mean = 1.08‰), and from –0.14‰ to 0.54‰ (mean = 0.18‰), respectively. By contrast, there is a narrow range of $\delta^{13}C_{org}$ values between –30.6‰ and –28.9‰ (mean = –29.8‰).

To correct for the influence of detrital Mo and U on isotopic compositions, the authigenic Mo and U isotope compositions of the black shales were calculated as follows ("auth" = authigenic, "bulk" = bulk or total sample, "det" = detrital).

$$\delta^{98}Mo_{auth} = \delta^{98}Mo_{bulk} - (Al/Mo)_{bulk} \times \{(\delta^{98}Mo_{det} - \delta^{98}Mo_{bulk}) / [(Al/Mo)_{det} - (Al/Mo)_{bulk}]\}$$

$$\delta^{238}U_{auth} = \delta^{238}U_{bulk} - (Al/U)_{bulk} \times \{(\delta^{238}U_{det} - \delta^{238}U_{bulk}) / [(Al/U)_{det} - (Al/U)_{bulk}]\}$$

For this calculation, the Mo (1.1 μg/g), U (2.7 μg/g), and Al (8.15 wt%) concentrations and the

Mo isotope (0.3‰), and U isotope (–0.3‰) compositions of the detrital fraction were assumed to be similar to average upper continental crust (Rudnick and Gao, 2013; Voegelin et al., 2014; Tissot and Dauphas, 2015; Noordmann et al., 2016; Willbold and Elliot, 2017). The $\delta^{98}Mo_{auth}$ and $\delta^{238}U_{auth}$ values for the Kettle Point black shales range from 0.55‰ to 2.05‰ (mean = 1.09‰), and from –0.29‰ to 0.60‰ (mean = –0.22‰), respectively. The difference between $\delta^{98}Mo_{auth}$ and $\delta^{98}Mo_{bulk}$ was minimal (≤0.03‰) whereas the difference between $\delta^{238}U_{auth}$ and $\delta^{238}U_{bulk}$ was larger (≤0.19‰), consistent with the lower U EFs compared to Mo EFs (see Figure 4).

The most distinctive observation of our isotopic dataset is the pronounced inverse correlation between $\delta^{98}Mo$ and $\delta^{238}U$ (Figure 6). A distinctive stratigraphic trend towards lower $\delta^{98}Mo$ values is observed from Unit 1 to Unit 4. By contrast, the opposite stratigraphic pattern is observed for $\delta^{238}U$ values, which progressively increase from Unit 1 to Unit 4 (Figure 4). The opposing stratigraphic trends in $\delta^{98}Mo$ and $\delta^{238}U$ do not closely follow Mo and U enrichment trends, consistent with the overall poor correlation between $\delta^{98}Mo$ and Mo EF, and between $\delta^{238}U$ and U EF (Figure 7). The plot of $\delta^{98}Mo$ versus Mo EF reveals two interesting features: 1) low $\delta^{98}Mo$ (<1‰) occurs over a wide range of Mo EFs, and 2) higher $\delta^{98}Mo$ (>1‰) is restricted to samples with lower Mo EFs. There is no statistically significant correlation between TOC content and either $\delta^{98}Mo$ or $\delta^{238}U$.

5. DISCUSSION

5.1. Elemental constraints on local depositional conditions for the Kettle Point black shales

The inverse correlation between the Mo and U isotope compositions of the Kettle Point black shales is the most significant feature of our geochemical dataset. Such a strong inverse

correlation has not been observed in the small number of pre-Cenozoic black shale units for which both Mo and U isotope data have been generated for the same samples (Asael et al., 2013; Kendall et al., 2015; Lu et al., 2017). To fully understand the significance of this inverse correlation between the Mo and U isotope compositions, we first use a combination of paleosalinity proxies, Fe-TOC-S systematics, redox-sensitive metal enrichments, and Mo/U ratios to constrain the local paleohydrographic and paleoredox conditions during deposition of the Kettle Point Formation in the Chatham Sag.

5.1.1. Paleosalinity: B/Ga, Sr/Ba, and TS/TOC ratios

Given the geological setting of the intracratonic Chatham Sag – a structural depression located between the Michigan and Appalachian basins – we examined the geochemical evidence for watermass salinity using three different elemental ratios. Specifically, we used B/Ga, Sr/Ba, and TS/TOC ratios to distinguish between marine, brackish, and freshwater conditions during deposition of the Kettle Point black shales (Wei et al., 2018; Wei and Algeo, in press).

Recently, Wei and Algeo (in press) used a compilation of data from modern fine-grained, carbonate-poor, siliciclastic sediments from modern environments to establish general thresholds for these water types. Sediments deposited in marine settings have the highest B/Ga (>6) and Sr/Ba (>0.5) ratios whereas sediments in brackish settings have intermediate B/Ga (3–6) and Sr/Ba (0.2–0.5) ratios and sediments in freshwater settings have the lowest B/Ga (<3) and Sr/Ba (<0.2) ratios. The accuracy of B/Ga ratios (~88%) as a paleosalinity proxy was shown to be greater than Sr/Ba ratios (~66%) for modern environments. Carbonate-bound Sr and the greater post-depositional mobility of the large ion lithophiles Sr and Ba can hamper efforts to use the Sr/Ba ratios of the fine-grained siliciclastic component (primarily clay minerals) of shales to distinguish between the

three water types. For black shales of the Kettle Point Formation, there is no statistically significant correlation between Sr/Ba ratios and TIC contents ($r = 0.18$, $p = 0.14$) and the TIC contents are low, suggesting that the bulk Sr/Ba ratios of the samples are largely controlled by the clay mineralogy composition. We do not observe clear evidence for excess biogenic Ba in the Kettle Point black shales based on a crossplot of Ba versus Al concentrations. However, post-depositional mobility of Sr and Ba remains a concern. The TS/TOC ratios can distinguish between freshwater (<0.1) and marine-brackish waters (>0.1) but cannot effectively distinguish between marine and brackish waters for ratios of 0.1–0.5 because in Phanerozoic marine and brackish environments the limiting factor on the extent of microbial sulfate reduction is typically the supply of organic carbon rather than sulfate. Higher TS/TOC ratios of >0.5 are more likely to indicate deposition from fully marine bottom waters. When applied in this fashion, the accuracy of the TS/TOC paleosalinity proxy was ~91% for modern environments (Wei and Algeo, in press).

We use these paleosalinity proxies to infer the depositional conditions for the black shales of the Kettle Point Formation (data are not reported for the grey-green mudstones, but these rocks were likely deposited during times of shallower sea-level in a more freshwater environment compared to the black shales; Bingham-Koslowski et al., 2016). The B/Ga proxy suggests that the black shales sampled from Units 1-2 were deposited from marine waters (B/Ga ratios >6) at higher sea-level. Unit 3 black shales may have been deposited from slightly brackish waters (B/Ga ratios near 6). The Unit 4 black shales were probably deposited from a more brackish watermass (B/Ga ratios typically <6) at lower sea-level. The TS/TOC ratios (>0.1) of the Unit 1-3 black shales are consistent with this interpretation, keeping in mind that ratios of 0.1–0.5 do not effectively discriminate between brackish and marine waters. The Sr/Ba ratios suggest deposition of Unit 1-2 black shales from both marine or brackish waters, Unit 3 black shales from brackish waters, and

Unit 4 black shales from brackish and freshwaters. Following Wei and Algeo (in press), we place more emphasis on the more robust B/Ga and TS/TOC paleosalinity proxies, which do not reveal evidence for dominance by freshwater inputs during Unit 4 deposition. Nevertheless, the B/Ga and Sr/Ba ratios show agreement in their overall stratigraphic trends and indicate that the Unit 4 black shales are most influenced by freshwater input into the Chatham Sag.

Based on lithological characteristics, Bingham-Koslowski et al. (2016) inferred that the black shales of Units 2 and 4 were deposited at times of higher eustatic sea-level compared to the black shales of Units 1 and 3 (see section 2). However, our paleosalinity estimates do not fully support this interpretation – our sampled Unit 4 black shales were deposited in the most brackish conditions. Unit 4 may capture the onset of a eustatic regression, which has also been inferred for the stratigraphically correlative upper Cleveland Member (Ohio Shale) in the Appalachian Basin based on trends in redox-sensitive elemental data and Mo/TOC ratios (Algeo et al., 2007; Algeo and Maynard, 2008). It is also noted that the overall stratigraphic trend towards lower B/Ga and Sr/Ba ratios of the sampled black shales do not capture the full story of sea-level changes for the entire Kettle Point Formation because our data only capture watermass conditions for the black shales specifically. The lithological variation in Units 1 and 3 (shallower-water grey-green mudstones and deeper-water black shales) still require significant sea-level changes within those units (Bingham-Koslowski et al., 2016).

5.1.2. Redox-sensitive metal constraints on local paleoredox and paleohydrographic conditions

The Kettle Point black shales were likely deposited in a redox-stratified basin with euxinic bottom waters based on Fe-TOC-S systematics. Organic carbon isotope compositions ($\delta^{13}C_{org}$ = –31‰ to –29‰) of the black shales are similar to other Upper Devonian black shales (including

those in the adjoining Michigan Basin and Appalachian Basin) and indicate a marine origin for the organic matter (Maynard, 1981; Hayes et al., 1999; Formolo et al., 2014), consistent with previous classification of the kerogen as predominantly Type I and II (Snowdon, 1984; Obermajer et al., 1997; Béland-Otis, 2013). A correlation between total Fe and total S contents ($r = 0.85$, $p < 0.001$; Figure 8A) suggests that much of the highly reactive Fe (i.e., Fe-bearing minerals that react with microbially-produced dissolved sulfide during deposition and early diagenesis) and TS was converted into pyrite. Well-correlated total Fe and TS contents are typically observed in other organic-sediments and black shales deposited from euxinic bottom waters (e.g., Raiswell and Berner, 1985; Dean and Arthur, 1989; Arthur and Sageman, 1994; Lyons et al., 2003; Scott et al., 2017). The Kettle Point black shales have consistently higher ratios of total Fe to TS relative to the pyrite Fe/S ratio of 0.87 (Figure 8A), likely reflecting the contribution of Fe from the siliciclastic detrital material. It is important to note that low Fe/Al ratios of most Kettle Point black shales, sometimes lower than the average upper crustal value of ~0.5 (Rudnick and Gao, 2003), are not contradictory to an interpretation of euxinic bottom waters. No correlation is observed between Fe and Al concentrations, indicating that the Fe abundances of the black shales are not controlled solely by detrital mineralogical variations. The Fe/Al ratio of detrital sediment delivered to the Chatham Sag may have been ≤0.35 based on the lowest Fe/Al ratios of the Kettle Point Formation (Figure 8B) and hence Fe/Al ratios above this threshold may reflect the authigenic Fe enrichments expected for euxinic depositional environments. It is also possible that the availability of reactive Fe was limited (Anderson and Raiswell, 2004; Lyons and Severmann, 2006; Raiswell et al., 2018). The poor correlation between TOC and TS (Figure 8C) indicates that the burial and preservation of the organic matter and sulfide in the Kettle Point Formation were decoupled and thus the amount of TS preserved is probably not a simple function of water column sulfide

concentrations but is also tied to reactive Fe availability (Scott et al., 2017). A peak in total S content and Fe/Al ratios around the Unit 1-2 boundary (Figure 4) suggests a transient increase in reactive Fe availability, possibly associated with a eustatic sea-level rise at this time (Bingham-Koslowski et al., 2016).

Additional evidence for euxinic bottom waters is the consistently high ratio of authigenic Mo to U enrichment in the Kettle Point black shales compared with modern seawater. The Mo and U EFs are tightly correlated ($r = 0.88$, $p < 0.001$) and most samples define a linear trend that is roughly equal to a Mo/U ratio of ~3 times modern seawater (Figure 9). This observation indicates that the accumulation rate of Mo substantially exceeded that of U, an expected characteristic of euxinic environments (Algeo and Tribovillard, 2009). At the lower Mo and U EFs observed for the Kettle Point Formation, there is no shift towards a steep downward trend suggestive of less intensely reducing (non-euxinic) conditions (Figure 9). None of the Kettle Point data plot along a trend of evolving water mass chemistry towards the low Mo/U ratios typical of a strongly restricted basin (Algeo and Tribovillard, 2009), indicating that there was significant communication between the waters of the Chatham Sag and the global ocean.

The Mo/U ratios of the Kettle Point black shales are higher than many other euxinic sediments and black shales and suggest an additional mechanism that promoted Mo enrichment in the Kettle Point Formation. Notably, similarly high Mo/U ratios occur in the modern Cariaco and Orca Basins. In these modern euxinic basins, the transfer of Mo to the lower water column is accelerated via adsorption of Mo to sinking Fe-Mn (oxyhydr)oxide particulates (Algeo and Tribovillard, 2009). When the Fe-Mn (oxyhydr)oxide particles are reduced and dissolved, Mo is released and subsequently is sequestered into organic matter and/or sulfide minerals. Compared to Mo, the affinity of U for Fe-Mn (oxyhydr)oxide particulates is significantly weaker (Hein and

Koschinsky, 2014), and hence U enrichments in black shales are not significantly affected by the flux of Fe-Mn (oxyhydr)oxide particulates (Algeo and Tribovillard, 2009). The strength of this particulate flux may have been strongest during deposition of upper Unit 4, which has the highest Mo concentrations, Mo/U EF ratios (>3 times the modern seawater ratio), and Mo/TOC ratios. This interpretation is further supported by the high V enrichments in upper Unit 4. In the modern ocean, V adsorbs to ferromanganese crusts more efficiently than Mo (Hein and Koschinsky, 2014) and Fe-Mn (oxyhydr)oxide particulates have been observed to enhance the V and Mo concentrations of modern anoxic sediments (Morford et al., 2005; Scholz et al., 2011).

Alternatively, the high Mo and V enrichments, Mo/TOC ratios, and Mo/U EF ratios in upper Unit 4 could reflect unusually high ("hyper-sulfidic") dissolved sulfide concentrations in the bottom waters. Scott et al. (2017) suggested that similarly high V enrichments in the Upper Devonian Bakken Shale (Williston Basin) require high dissolved sulfide concentrations (> 8 mM) to enable the efficient reduction of V(IV) to V(III) and high burial rates of V in euxinic sediments. Because modern euxinic basins do not have sediments with V hyper-enrichments (defined as >500 μg/g by Scott et al., 2017) like those observed in these Upper Devonian black shales, the minimum dissolved sulfide concentration necessary to enable V hyper-enrichments in euxinic sediments was proposed by Scott et al. (2017) to be >8 mM, which is the highest dissolved sulfide concentration observed in modern marine euxinic basins (from the Framvaren Fjord; Skei et al., 1988). Because modern analogs for V hyper-enrichments are absent, it is difficult to test this hypothesis. However, we note that the Unit 4 samples with V hyper-enrichments are characterized by a wide range of Mo enrichments (including several examples of Mo concentrations between 46 and 100 μg/g), which is not consistent with hyper-sulfidic conditions. Black shales from the Ediacaran Doushantuo Formation (South China) have V hyper-enrichments in non-euxinic samples with

lower Mo concentrations (<15 μg/g) (Ostrander et al., 2019) than those found in upper Unit 4 of the Kettle Point Formation. Hence, hyper-sulfidic water column and pore water conditions may not be required to produce V hyper-enrichments in black shales.

Our preferred interpretation is that a strong Fe-Mn particulate flux across a deep-water chemocline (i.e., euxinic waters did not extend far above the sediment-water interface) caused the high Mo and V enrichments in the upper part of Unit 4. We speculate that the presence of V hyper-enrichments in black shales from the intracratonic Chatham Sag, but not in the modern continental margin Cariaco and Orca Basins, can be explained by differences in hydrographic conditions. During Unit 4 time, the chemocline in the Chatham Sag may have moved to an overall deeper position in the water column as a result of lower eustatic sea-level, as suggested by the paleosalinity evidence for more brackish conditions during black shale deposition in Unit 4. Changes in ocean circulation patterns and/or more localized events such as increased wind speeds can cause transient inflows of oxygenated marine waters and deepen the pycnocline (e.g., Scholz et al., 2011, 2013; Ostrander et al., 2019). The intermittent presence of marcasite in Kettle Point black shales from other sections (including Unit 4) within the Chatham Sag (Delitala, 1984; Armstrong and Carter, 2010; Béland-Otis, 2013) may suggest transient deep-water oxygenation events where dissolved O_2 penetrated briefly into sediments (Schieber, 2011). A deep-water, fluctuating chemocline situated close to the sediment-water interface allows a strong flux of Fe-Mn (oxyhydr)oxides that survive transport through the euxinic bottom waters to the sediment-water interface. Reductive dissolution of Fe-Mn (oxyhydr)oxides in euxinic sediments may increase the efficiency of Mo and V burial in those sediments because less Mo and V are recycled back into the water column (cf. Algeo and Tribovillard, 2009). Lower Mo and V enrichments in Units 1-3 and lower Unit 4 may reflect a shallower-water chemocline, below which a greater

proportion of sinking Fe-Mn (oxyhydr)oxides dissolved in the euxinic water column and thus recycled their trace metals farther up in the water column.

A further implication of our data is that the strength of an Fe-Mn particulate flux can affect the ability of Mo/TOC ratios to infer the degree of local basin restriction from the open ocean. The highest Mo/TOC ratios during upper Unit 4 deposition could be construed as evidence for higher sea-level and thus increased water-mass exchange between the local basin and open ocean (cf. Algeo and Lyons, 2006). However, this interpretation conflicts with the paleosalinity evidence (B/Ga ratios) for typically brackish conditions and thus lower sea-level during Unit 4 black shale deposition. Despite the apparently more restricted conditions that should be caused by lower sea-level, higher Mo/TOC ratios were preserved in the upper Unit 4 black shales because of the enhanced delivery of Mo to the euxinic sediments by a strong Fe-Mn particulate flux. Hence, the influence of an Fe-Mn particulate flux should be considered when using Mo/TOC ratios to infer the extent of local sedimentary basin restriction from the open ocean.

5.2. Significance of the inverse Mo-U isotope correlation for the Kettle Point Formation

5.2.1. Changes in local depositional conditions as a driver of anti-correlated Mo-U isotope variations in euxinic black shales

It is not likely that the opposite stratigraphic trends in the Mo and U isotope compositions of the Kettle Point black shales arise from changes in global ocean redox conditions based on our knowledge of Mo and U isotope fractionation in modern marine environments.

In the modern oceans, the lighter Mo isotopes are always preferentially removed from seawater to sediments, with the magnitude of Mo isotope fractionation depending on local redox

conditions (modern global seawater δ^{98}Mo = 2.34 ± 0.10‰; Barling et al., 2001; Siebert et al., 2003; Nakagawa et al., 2012; Nägler et al., 2014). The largest Mo isotope fractionation of ~3‰ occurs between seawater and ferromanganese crusts and nodules in well-oxygenated marine environments (Barling et al., 2001; Siebert et al., 2003; Barling and Anbar, 2004; Wasylenki et al., 2008; Poulson Brucker et al., 2009). By contrast, Mo isotope fractionation in weakly oxygenated, anoxic/non-sulfidic, and euxinic settings is commonly <1‰ (except in some weakly euxinic settings; Barling et al., 2001; Arnold et al., 2004; Poulson et al., 2006; Siebert et al., 2006; Poulson Brucker et al., 2009; Nägler et al., 2011; Goldberg et al., 2012; Noordmann et al., 2015; Andersen et al., 2018; Bura-Nakić et al., 2018). An expansion of ocean euxinia will decrease the extent to which lighter Mo isotopes are removed to sediments, thus shifting the global seawater δ^{98}Mo to lower values (Barling et al., 2001; Arnold et al., 2004).

For U isotopes, the largest isotope fractionation between modern global seawater (–0.39 ± 0.02 ‰; Stirling et al., 2007; Weyer et al., 2008; Tissot and Dauphas, 2015; Andersen et al., 2014, 2016) and sediments occurs in euxinic basins and results in preferential burial of the heavier ^{238}U isotope in euxinic sediments, with fractionations typically exceeding 0.4‰ (Stirling et al., 2007; Weyer et al., 2008; Kaltenbach, 2013; Andersen et al., 2014; Holmden et al., 2015; Noordmann et al., 2015; Rolison et al., 2017; Bura-Nakić et al., 2018). The magnitude of U isotope fractionation is generally smaller in all other marine sinks (Stirling et al., 2007; Weyer et al., 2008; Brennecka et al., 2011a; Romaniello et al., 2013; Goto et al., 2014; Tissot and Dauphas, 2015; Andersen et al., 2016; Noordmann et al., 2016; Wang et al., 2016; Chen et al., 2016, 2018; Tissot et al., 2018). Hence, an expansion of ocean euxinia would deplete the global ocean reservoir of ^{238}U, resulting in lower global seawater δ^{238}U (Weyer et al., 2008; Montoya-Pino et al., 2010).

In summary, global ocean redox changes will shift global seawater δ^{98}Mo and δ^{238}U in the same direction. It follows that if global redox variations were the dominant control on the stratigraphic Mo-U isotope trends of the euxinic Kettle Point black shales, then parallel (i.e., positively correlated) stratigraphic trends should be observed for the two isotope systems. Hence, the local depositional environment must have been the major control on the Mo-U isotope systematics of black shales in the Kettle Point Formation. Recent studies have demonstrated that variations in the local depositional environment of modern euxinic basins (Black Sea and Cariaco Basin) can drive inverse correlations between the Mo and U isotope compositions of euxinic sediments (Brüske et al., in press). Changes in wind and thermohaline ocean circulation patterns and freshwater inputs may have caused the inverse correlation between δ^{98}Mo and δ^{238}U for the S5 sapropel in the Eastern Mediterranean Sea (Andersen et al., 2018). Hence, the inverse correlation between δ^{98}Mo and δ^{238}U for the Kettle Point black shales is most likely explained by changes in the local depositional environment of the Chatham Sag.

There are likely multiple local depositional factors affecting the Mo and U isotope compositions of the Kettle Point black shales because no single local depositional redox indicator (e.g., Fe/Al ratios, TOC content, TS content, redox-sensitive metal enrichments, Mo/TOC ratios, Mo/U ratios) exhibits a strong correlation with both Mo and U isotope compositions. In section 5.1, evidence was presented for a strong Fe-Mn (oxyhydr)oxide particulate flux to the sediments during deposition of the upper Kettle Point Formation (see section 5.1). Hence, we consider the impact of changes in local paleohydrographic and paleoredox conditions on the metal isotope compositions of black shales throughout the Kettle Point Formation as well as the impact of the Fe-Mn (oxyhydr)oxide particulate flux on the metal isotope compositions of V-rich samples (EF >5) above ~57 m depth in Unit 4 (Figure 4). As the anti-correlated Mo and U isotope

systematics can be defined using the entire dataset, we examine processes capable of influencing the isotope composition of both metals in black shales.

5.2.2. Influence of bottom water sulfide concentrations and sea-level changes (Units 1-4)

Changes in bottom-water sulfide concentrations can explain the inverse Mo-U isotope correlation of the Kettle Point black shales because such changes influence the magnitude of local Mo and U isotope fractionation between seawater and the underlying sediments. In modern euxinic environments, the magnitude of Mo isotope fractionation between euxinic sediments and seawater is small when bottom-water sulfide concentrations are sufficiently high ($[H_2S]_{aq}$ >11 μM) to promote near-quantitative conversion of molybdate to the most particle-reactive tri- and tetra-thiomolybdates and there is also near-quantitative removal of Mo from the bottom waters to sediments (Barling et al., 2001; Arnold et al., 2004; Neubert et al., 2008; Nägler et al., 2011; Noordmann et al., 2015; Bura-Nakić et al., 2018; Brüske et al., in press). Under such conditions, the δ^{98}Mo of the sediments approaches global seawater δ^{98}Mo. By contrast, non-quantitative tri- and tetra-thiomolybdate formation coupled with non-quantitative Mo removal from weakly sulfidic ($[H_2S]_{aq}$ <11 μM) bottom waters causes significant Mo isotope fractionation (up to 3‰), resulting in the preferential removal of lighter Mo isotopes from the water column to sediments. Consequently, euxinic sediments deposited from local weakly euxinic bottom waters have lower δ^{98}Mo compared to euxinic sediments deposited from local strongly euxinic bottom waters. Hence, we infer that the sampled black shales of Unit 1 and lower Unit 2 were deposited from more sulfidic bottom waters compared to the interval from upper Unit 2 to Unit 4. The Kettle Point U isotope data are consistent with a control by bottom-water sulfide concentrations. In modern euxinic settings, more sulfidic conditions generally favor greater drawdown of U from bottom and pore

waters, resulting in a smaller U isotope fractionation and lower $\delta^{238}U$ in euxinic sediments, although factors such as basin geometry and deep-water renewal rates are also important controls. By contrast, larger U isotope fractionations can occur in weakly euxinic settings, resulting in euxinic sediments with higher $\delta^{238}U$ (Andersen et al., 2018; Bura-Nakić et al., 2018; Brüske et al., in press).

Variations in sea-level were likely a driving force behind changes in bottom-water sulfide concentrations and thus the inverse Mo-U isotope correlation of the Kettle Point black shales. Statistically significant correlations are observed between each metal isotope system and the paleosalinity indicators, particularly B/Ga ratios (Figure 10). Times of relatively lower sea-level (more brackish conditions) are inferred to be associated with a deeper water-column chemocline and lower bottom water sulfide concentrations. For these conditions, non-quantitative removal of Mo and U to the euxinic sediments may have led to preferential removal of lighter Mo isotopes and heavier U-238 such that lower $\delta^{98}Mo$ and higher $\delta^{238}U$ were preserved in the black shales. By contrast, times of relatively higher sea-level (more marine conditions) were associated with a shallower water-column chemocline and higher bottom water sulfide concentrations. Hence, more quantitative removal of Mo and U from bottom waters to the euxinic sediments may have enabled the preservation of higher $\delta^{98}Mo$ and lower $\delta^{238}U$ in the black shales.

Changes in freshwater-seawater mixing ratios are not likely to explain the inverse correlation between the Mo and U isotope compositions of the Kettle Point black shales. If the Late Devonian ocean had only a mildly greater extent of seafloor anoxia and euxinia compared to the modern ocean (White et al., 2018), then the Late Devonian seawater Mo concentrations were probably not significantly lower than the modern ocean. The Mo and U concentrations of oceanic inputs (rivers and groundwater) to the Late Devonian ocean were thus probably an order of

magnitude lower than seawater concentrations like today (Anderson, 1987; Emerson and Huested, 1991; Dunk et al., 2002; Miller et al., 2011). Large variations in freshwater-seawater mixing ratios would thus be required to drive the large anti-correlated variations in δ^{98}Mo and δ^{238}U observed for the Kettle Point black shales. However, there is no evidence for severe basin restriction from our elemental data (e.g., consistently high Mo/U ratios in black shales throughout the Kettle Point Formation). Most importantly, the highest δ^{238}U values in the Kettle Point Formation are observed in the more brackish Unit 4 black shales and these δ^{238}U values are the most isotopically distinct from the average δ^{238}U of modern rivers (~ –0.3‰; Tissot and Dauphas, 2015; Andersen et al., 2016; Noordmann et al., 2016). Riverine inputs are thus clearly not a major control on the δ^{238}U of the Kettle Point black shales. Although the δ^{98}Mo values in the brackish Unit 4 black shales are close to the modern riverine average (0.3-0.7‰; Archer and Vance, 2008; King and Pett-Ridge, 2018), Herrmann et al. (2012) showed that unrealistically high freshwater-seawater ratios are required to enable riverine inputs to appreciably change the Mo isotope compositions of black shales deposited in the Late Pennsylvanian Midcontinent Sea. Hence, bottom water sulfide concentrations (and thus the efficiency of metal removal from bottom waters) are more likely than freshwater-seawater mixing ratios to explain the inverse correlation between δ^{98}Mo and δ^{238}U for the Kettle Point black shales.

5.2.3. Influence of the Fe-Mn (oxyhydr)oxide particulate flux (upper Unit 4)

The δ^{98}Mo and δ^{238}U of the V-rich samples from upper Unit 4 may be explained by a combination of a strong Fe-Mn (oxyhydr)oxide particulate flux and non-quantitative removal of Mo and U from weakly euxinic bottom waters. These Mo- and V-rich samples are characterized by consistently low δ^{98}Mo (0.5-1.0‰), which is consistent with delivery of isotopically light Mo

to the euxinic sediments by Fe-Mn particulates (Figure 11; Bura-Nakić et al., 2018; Scholz et al., 2013, 2018; Ostrander et al., 2019; Brüske et al., in press). However, within Unit 4, the magnitude of V enrichments does not correlate with δ^{98}Mo, suggesting that another factor, specifically the dissolved sulfide concentrations of the weakly euxinic bottom waters, was also an important influence on the δ^{98}Mo of Unit 4. It is not likely that hyper-sulfidic conditions (an alternative explanation for high V enrichments in black shales; Scott et al., 2017) caused the low δ^{98}Mo values in upper Unit 4. Such conditions would be expected to promote quantitative conversion of molybdate to tetrathiomolybdate, resulting in a small Mo isotope fractionation between the water column and the euxinic sediments (≤0.5‰; Nägler et al., 2011; Bura-Nakić et al., 2018). Hence, hyper-sulfidic conditions should cause higher δ^{98}Mo in the Unit 4 black shales, but this is not observed.

The δ^{238}U of the upper Unit 4 samples was probably not affected significantly by this particulate flux given the weak affinity of U for Fe-Mn (oxyhydr)oxides. It is also noted that such particulates would be expected to deliver isotopically lighter U to the sediments (Brennecka et al., 2011a; Goto et al., 2014; Wang et al., 2016) but the Unit 4 samples have the highest δ^{238}U observed in the Kettle Point Formation. These unusually high δ^{238}U values (0.4-0.6‰) likely reflect a large U isotope fractionation during U sequestration into the sediments deposited from weakly euxinic bottom waters. The minimum U isotope fractionation during Unit 4 deposition was 0.8-1.0‰ given that Famennian seawater δ^{238}U was probably lower than modern seawater δ^{238}U (Meyer and Kump, 2008; White et al., 2018; also see section 5.3). This estimate for the U isotope fractionation approaches the full expression of abiotic and biotic U isotope fractionation during U(VI) reduction to U(IV) (~1.0-1.2‰) and clearly reflects incomplete removal of U from bottom- and pore-waters (Basu et al., 2014; Andersen et al., 2014; Stirling et al., 2015; Stylo et al., 2015; Rolison et al.,

2017; Brown et al., 2018). It has been observed that large U isotope fractionations are associated with U(VI) reduction to U(IV) in the hyper-sulfidic Framvaren Fjord (Kaltenbach, 2013). However, we do not currently favor hyper-sulfidic conditions as an explanation for the geochemical characteristics of the upper Unit 4 black shales because such conditions should have promoted the preservation of high δ^{98}Mo in these rocks, which is not observed.

Overall, the Mo/U ratios and Mo-U isotope data for the V-rich Unit 4 black shales suggest a deep and possibly fluctuating water-column chemocline (Algeo and Tribovillard, 2009), underlain by weakly euxinic bottom waters, across which a strong flux of Fe-Mn (oxyhydr)oxides delivered V and isotopically light Mo to the sediments. Contemporaneously, the weakly euxinic conditions promoted enrichment of heavy U-238 in the sediments. In summary, variations in bottom water sulfide concentrations (influenced by sea-level changes) may have been the dominant controlling mechanism that drove the strong inverse correlation between the δ^{98}Mo and δ^{238}U of the black shales from the Kettle Point Formation.

5.2.4. Implications for the use of Mo and U isotopes as global ocean paleoredox proxies

The inverse correlation between the Mo and U isotope compositions of the Kettle Point black shales highlights the danger of relying on a single metal isotope system to interpret stratigraphic trends within a euxinic black shale unit. When there is a clear change in local redox conditions (e.g., from oxic to euxinic) identified by elemental data, it is relatively straightforward to avoid misinterpretation of stratigraphic trends, as shown by studies of Mesozoic oceanic anoxic events (e.g., Pearce et al., 2008; Westermann et al., 2014; Goldberg et al., 2016; Dickson et al., 2016, 2017). However, if local redox conditions were predominantly euxinic, it is more challenging to interpret stratigraphic trends in the Mo and U isotope compositions of black shales.

Without careful consideration of local depositional effects on isotope systematics, the stratigraphically upward decreasing trend in δ^{98}Mo may have been misinterpreted as a significant global expansion of ocean euxinia instead of a local change in bottom water sulfide concentrations. By contrast, if the U isotope data had been used in isolation, then the stratigraphically upward increasing trend in δ^{238}U may have been misinterpreted as a large decrease in the extent of ocean euxinia. The inverse correlation between Mo and U isotopes indicates that neither interpretation is correct. In further support of this interpretation, we note that stratigraphic trends in the U isotope composition of the Lower Famennian black shales of the Kettle Point Formation do not mimic the minor changes in global seawater δ^{238}U inferred for this time from the stratigraphic trends in carbonate δ^{238}U of the Devil's Gate Formation, Nevada (White et al., 2018). While our data do not preclude small variations in the global extent of oxic, anoxic, and euxinic conditions in the oceans during deposition of the Kettle Point Formation, the inverse correlation between Mo and U isotopes requires that the dominant control on the stratigraphic trends was changes in the local depositional environment. Despite this inverse correlation, it is still possible to make inferences about the Mo and U isotope compositions of global Famennian seawater, as discussed below.

5.3. Global seawater Mo and U isotope compositions during the Famennian

As observed in modern euxinic environments (Bura-Nakić et al., 2018; Brüske et al., in press), the highest authigenic δ^{98}Mo (2.0‰) and lowest authigenic δ^{238}U (–0.3‰) values from the Kettle Point Formation place minimum and maximum constraints on global seawater Mo and U isotope compositions during the Early Famennian. The isotopic offset between black shale and seawater metal isotopic compositions can be difficult to constrain precisely, but in this case, the inverse correlation between δ^{98}Mo and δ^{238}U for the Kettle Point black shales provides a key clue.

Notably, the slope of the regression line for the Kettle Point Formation on a crossplot of δ^{98}Mo versus δ^{238}U is similar to the slope of the inverse correlation for modern euxinic basins (Saanich Inlet, Cariaco Basin, Kyllaren Fjord, and Lake Rogoznica; Bura-Nakić et al., 2018) but is slightly offset to lower values (Figure 12). This observation suggests that the Famennian seawater isotope compositions of Mo and U were somewhat lower compared to the modern global seawater values of 2.34 ± 0.10 ‰ and –0.39 ± 0.02‰, respectively. Hence, the extent of Famennian ocean euxinia was somewhat greater than today, consistent with the widespread paleogeographic distribution of Famennian black shales in epicontinental seas (White et al., 2018).

This interpretation is consistent with previous estimates for global seawater δ^{238}U and δ^{98}Mo. An average global Late Devonian seawater δ^{238}U of about –0.7‰ was inferred from carbonate data spanning the Frasnian-Famennian boundary in the Devil's Gate Formation of Nevada and the Baisha section of South China (this average was calculated by assuming a typical offset of 0.3‰ between the carbonates and global seawater δ^{238}U; Song et al., 2017; Chen et al., 2018; Tissot et al., 2018; White et al., 2018). A minimum seawater δ^{98}Mo value of ~1.9‰ was inferred from the highest δ^{98}Mo value from the Frasnian-Famennian Chattanooga Shale (Dahl et al., 2010). Extrapolation of the linear regression between δ^{98}Mo and δ^{238}U for the Kettle Point Formation (Figure 12) suggests a global seawater δ^{98}Mo of ~2.0-2.2‰ when global seawater δ^{238}U is –0.7‰ to –0.4‰. Because the Frasnian-Famennian boundary is near the base of the Kettle Point Formation in the Gore of Chatham core, we make no effort here to evaluate the extent or impact of ocean euxinia on the Kellwasser extinction events.

A second constraint on later Famennian seawater δ^{238}U can be placed using the highest δ^{238}U values (0.5-0.6‰) from Unit 4. The maximum U isotope fractionation for biotic and abiotic reduction of U(VI) to U(IV) is ~1.0-1.2‰ (Basu et al., 2014; Andersen et al., 2014; Stirling et al.,

2015; Stylo et al., 2015; Rolison et al., 2017; Brown et al., 2018). Hence, Late Famennian seawater $\delta^{238}U$ during upper Unit 4 deposition is inferred to be –0.7‰ to –0.4‰ if the full magnitude of U isotope fractionation was expressed during deposition of these shales. If the magnitude of U isotope fractionation was smaller, then global seawater $\delta^{238}U$ during the Late Famennian would be higher than modern global seawater, implying a globally more oxygenated Late Famennian ocean. However, this scenario is not consistent with the widespread paleogeographic distribution of Famennian black shales. Hence, we infer that the full expression of U isotope fractionation during U(VI) reduction to U(IV) can occur in intracratonic marine environments despite the scarcity of such large U isotope fractionations in modern euxinic basins.

In summary, our Mo and U isotope data suggest that the Famennian ocean had an overall greater extent of euxinic waters compared to the modern ocean. Previously published isotope mass-balance models suggest that for seawater $\delta^{98}Mo$ and $\delta^{238}U$ values of 2.0‰ and –0.7‰, respectively, the extent of euxinic seafloor was likely <5% of the global ocean (Goldberg et al., 2016; Gilleaudeau et al., 2019). Hence, euxinic waters were likely confined to continental margins and epicontinental basins during the Famennian.

6. CONCLUSIONS

The geochemical data from the euxinic black shales of the Kettle Point Formation highlight the importance of an integrated geochemical approach to correctly interpret stratigraphic trends in Mo and U isotope data. Classical interpretation of the black shale Mo and U isotope data would have yielded contradictory findings of expanded ocean euxinia and contracted ocean euxinia based on the observed stratigraphic trends towards lower $\delta^{98}Mo$ and

higher $\delta^{238}U$ upsection in the Kettle Point Formation. Our findings raise the possibility that incorrect interpretations of global ocean redox conditions could occur if only one metal isotope system (either Mo or U) was applied to a euxinic black shale unit. The inverse correlation between the Mo and U isotope compositions of the Kettle Point black shales is similar to that observed for modern euxinic sediments and is best explained by physico-chemical changes to the local depositional environment (particularly changes in bottom-water sulfide concentrations and efficiency of metal burial in sediments) driven by sea-level variations. Consistent with previous studies, the Mo and U isotope data from the Kettle Point Formation suggest that the extent of global ocean euxinia in the Famennian ocean was greater than today but was likely <5% of the seafloor, indicating that euxinic seafloor was likely confined to epicontinental basins and along continental margins.

Acknowledgements

This study was supported by a NSERC Discovery Grant (grant number RGPIN-435930) and an Ontario Early Researcher Award to BK. The Metal Isotope Geochemistry Laboratory at Waterloo was funded by the Canada Foundation for Innovation, Ontario Research Fund, and University of Waterloo. DJO and YB acknowledge funding from NSF-GEOS (grant number 1458514) and the Geneseo Foundation. Charles Wu is acknowledged for assistance with total organic carbon and total sulfur measurements. Catherine Beland-Otis provided valuable advice on a suitable drill core for this study. Emily Hauf assisted with the collection of conodonts. Jordan Clark is thanked for coordinating sampling at the Ontario Oil, Gas and Salt Resources Library in London, Ontario. The authors thank guest editor Thomas Algeo, reviewer Geoff Gilleaudeau, and two anonymous reviewers for their helpful comments and suggestions that improved the paper.

REFERENCES

Abe M., Suzuki T., Fujii Y., Hada M. and Hirao K. (2008) An *ab initio* molecular orbital study of the nuclear volume effects in uranium isotope fractionations. *Journal of Chemical Physics* **129**, 164309.

Algeo T. J. and Lyons T. W. (2006) Mo–total organic carbon covariation in modern anoxic marine environments: Implications for analysis of paleoredox and paleohydrographic conditions. *Paleoceanography* **21**, PA1016.

Algeo T. J. and Tribovillard N. (2009) Environmental analysis of paleoceanographic systems based on molybdenum–uranium covariation. *Chemical Geology* **268**, 211-225.

Algeo T. J. and Maynard J. B. (2008) Trace-metal covariation as a guide to water-mass conditions in ancient anoxic marine environments. *Geosphere* **4**, 872-887.

Algeo T. J., Lyons T. W., Blakey R. C. and Over D. J. (2007) Hydrographic conditions of the Devono–Carboniferous North American Seaway inferred from sedimentary Mo–TOC relationships. *Palaeogeography, Palaeoclimatology, Palaeoecology* **256**, 204-230.

Andersen M. B., Romaniello S., Vance D., Little S. H., Herdman R. and Lyons T. W. (2014) A modern framework for the interpretation of $^{238}U/^{235}U$ in studies of ancient ocean redox. *Earth and Planetary Science Letters* **400**, 184-194.

Andersen M. B., Vance D., Morford J. L., Bura-Nakić E., Breitenbach S. F. M. and Och L. (2016) Closing in on the marine $^{238}U/^{235}U$ budget. *Chemical Geology* **420**, 11-22.

Andersen M. B., Stirling C. H. and Weyer S. (2017) Uranium isotope fractionation. *Reviews in Mineralogy and Geochemistry* **82**, 799-850.

Andersen M. B., Matthews A., Vance D., Bar-Matthews M., Archer C. and de Souza G. F. (2018) A 10-fold decline in the deep Eastern Mediterranean thermohaline overturning circulation during the last interglacial period. *Earth and Planetary Science Letters* **503**, 58-67.

Anderson R. F. (1987) Redox behavior of uranium in an anoxic marine basin. *Uranium* **3**, 145-164.

Anderson T. F. and Raiswell R. (2004) Sources and mechanisms for the enrichment of highly reactive iron in euxinic Black Sea sediments. *American Journal of Science* **304**, 203-233.

Archer C. and Vance D. (2008) The isotopic signature of the global riverine molybdenum flux and anoxia in the ancient oceans. *Nature Geoscience* **1**, 597-600.

Ardakani O. H., Chappaz A., Sanei H. and Mayer B. (2016) Effect of thermal maturity on remobilization of molybdenum in black shales. *Earth and Planetary Science Letters* **449**, 311-320.

Armstrong D. K. and Carter T. R. (2010). The subsurface Paleozoic stratigraphy of southern Ontario. *Ontario Geological Survey Special Volume 7.*

Armstrong D. K. and Dodge J. E. P. (2007). Paleozoic geology of southern Ontario. *Ontario Geological Survey, Miscellaneous Release—Data 219.*

Armstrong D. K. (1986) Trace element geochemistry and petrology of the Kettle Point Formation (Upper Devonian), a black shale unit of southwestern Ontario. MSc thesis, University of Waterloo.

Arnold G. L., Anbar A. D., Barling J. and Lyons T. W. (2004) Molybdenum isotope evidence for widespread anoxia in mid-Proterozoic oceans. *Science* **304**, 87-90.

Arthur M. A. and Sageman B. B. (1994) Marine black shales: depositional mechanisms and environments of ancient deposits. *Annual Reviews of Earth and Planetary Sciences* **22**, 499-551.

Asael D., Tissot F. L. H., Reinhard C. T., Rouxel O., Dauphas N., Lyons T. W., Ponzevera E., Liorzou C. and Chéron S. (2013) Coupled molybdenum, iron and uranium stable isotopes as oceanic paleoredox proxies during the Paleoproterozoic Shunga Event. *Chemical Geology* **362**, 193-210.

Barling J. and Anbar A. D. (2004) Molybdenum isotope fractionation during adsorption by manganese oxides. *Earth and Planetary Science Letters* **217**, 315-329.

Barling J., Arnold G. L. and Anbar A. D. (2001) Natural mass-dependent variations in the isotopic composition of molybdenum. *Earth and Planetary Science Letters* **193**, 447-457.

Basu A., Sanford R. A., Johnson T. M., Lundstrom C. C. and Löffler F. E. (2014) Uranium isotopic fractionation factors during U(VI) reduction by bacterial isolates. *Geochimica et Cosmochimica Acta* **136**, 100-113.

Béland Otis C. (2013) Gas assessment of the Devonian Kettle Point Formation. *Ontario Geological Survey*, Open File Report 6279.

Biegeleisen J. (1996) Nuclear Size and Shape Effects in Chemical Reactions. Isotope Chemistry of the Heavy Elements. *Journal of the American Chemical Society* **118**, 3676-3680.

Bingham-Koslowski N., Tsujita C., Jin J. and Azmy K. (2016) Widespread Late Devonian marine anoxia in eastern North America: a case study of the Kettle Point Formation black shale, southwestern Ontario. *Canadian Journal of Earth Sciences* **53**, 837-855.

Brennecka G. A., Wasylenki L. E., Bargar J. R., Weyer S. and Anbar A. D. (2011a) Uranium isotope fractionation during adsorption to Mn-oxyhydroxides. *Environmental Science and Technology* **45**, 1370-1375.

Brennecka G. A., Herrmann A. D., Algeo T. J. and Anbar A. D. (2011b). Rapid expansion of oceanic anoxia immediately before the end-Permian mass extinction. *Proceedings of the National Academy of Sciences USA* **108**, 17631-17634.

Brown S. T., Basu A., Ding X., Christensen J. N. and DePaolo D. J. (2018) Uranium isotope fractionation by abiotic reductive precipitation. *Proceedings of the National Academy of Sciences USA* **115**, 8688-8693.

Brüske A., Weyer S., Zhao M.-Y., Planavsky N. J., Wegwerth A., Neubert N., Dellwig O., Lau K. V. and Lyons T. W. (in press) Correlated molybdenum and uranium isotope signatures in modern anoxic sediments: Implications for their use as paleo-redox proxy. *Geochimica et Cosmochimica Acta*. DOI: https://doi.org/10.1016/j.gca.2019.11.031.

Bura-Nakić E., Andersen M. B., Archer C., de Souza G. F., Marguš M. and Vance D. (2018) Coupled Mo-U abundances and isotopes in a small marine euxinic basin: Constraints on processes in euxinic basins. *Geochimica et Cosmochimica Acta* **222**, 212-229.

Chen X., Romaniello S. J., Herrmann A. D., Wasylenki L. E. and Anbar A. D. (2016) Uranium Isotope Fractionation During Coprecipitation with Aragonite and Calcite. *Geochimica et Cosmochimica Acta* **188**, 189-207.

Chen X., Romaniello S. J., Herrmann A. D., Hardisty D., Gill B. C. and Anbar A. D. (2018) Diagenetic effects on uranium isotope fractionation in carbonate sediments from the Bahamas. *Geochimica et Cosmochimica Acta* **237**, 294-311.

Crusius J. and Thomson J. (2000) Comparative behavior of authigenic Re, U, and Mo during reoxidation and subsequent long-term burial in marine sediments. *Geochimica et Cosmochimica Acta* **64**, 2233-2242.

Dahl T. W., Hammarlund E. U., Anbar A. D., Bond D. P. G., Gill B. C., Gordon G. W., Knoll A. H., Nielsen A. T., Schovsbo N. H. and Canfield D. E. (2010) Devonian rise in atmospheric oxygen correlated to the radiations of terrestrial plants and large predatory fish. *Proceedings of the National Academy of Sciences* **107**, 17911-17915.

Dahl T. W., Canfield D. E., Rosing M. T., Frei R. E., Gordon G. W., Knoll A. H. and Anbar A. D. (2011) Molybdenum evidence for expansive sulfidic water masses in ~750 Ma oceans. *Earth and Planetary Science Letters* **311**, 264-274.

Dean W. E. and Arthur M. A. (1994) Iron-sulfur-carbon relationships in organic-carbon-rich sequences I: Cretaceous Western Interior Seaway. *American Journal of Science* **289**, 708-743.

Delitala F. (1984) The mineralogy and geochemistry of the Kettle Point oil shale, S.W. Ontario. MSc thesis, University of Western Ontario.

Dickson A. J., Jenkyns H. C., Porcelli D., van den Boorn S. and Idiz E. (2016) Basin-scale controls on the molybdenum-isotope composition of seawater during Oceanic Anoxic Event 2 (Late Cretaceous). *Geochimica et Cosmochimica Acta* **178**, 291-306.

Dickson A. J., Gill B. C., Ruhl M., Jenkyns H. C., Porcelli D., Idiz E., Lyons T. W. and van den Boorn S. H. J. M. (2017) Molybdenum-isotope chemostratigraphy and paleoceanography of the Toarcian Oceanic Anoxic Event (Early Jurassic). *Paleoceanography* **32**, 813-829.

Dickson A. J., Idiz E., Porcelli D. and van den Boorn S.H.J.M. (in press) The influence of thermal maturity on the stable isotope compositions and concentrations of molybdenum,

zinc, and cadmium in organic-rich marine rocks. *Geochimica et Cosmochimica Acta*. DOI: https://doi.org/10.1016/j.gca.2019.11.001.

Dunk R. M., Mills R. A. and Jenkins W. J. (2002) A revaluation of the oceanic uranium budget for the Holocene. *Chemical Geology* **190**, 45-67.

Emerson S. R. and Huested S. S. (1991) Ocean anoxia and the concentration of molybdenum and vanadium in seawater. *Marine Chemistry* **34**, 177-196.

Ettensohn F. R. (1985) Controls on development of Catskill Delta complex basin-facies. In: Woodrow D. L. and Sevon W. D. (Eds.), The Catskill Delta. *Geological Society of America Special Paper 201*, pp. 65-77.

Formolo M. J., Riedinger N. and Gill B. C. (2014) Geochemical evidence for euxinia during the Late Devonian extinction events in the Michigan Basin (U.S.A). *Palaeogeography, Palaeoclimatology, Palaeoecology* **414**, 146-154.

Gilleaudeau G. J., Romaniello S. J., Luo G., Kaufman A. J., Zhang F., Klaebe R. M., Kah L. C., Azmy K., Bartley J. K., Zheng W., Knoll A. H. and Anbar A. D. (2019) Uranium isotope evidence for limited euxinia in mid-Proterozoic oceans. *Earth and Planetary Science Letters* **521**, 150-157.

Goldberg T., Archer C., Vance D., Thamdrup B., McAnena A. and Poulton S. W. (2012) Controls on Mo isotope fractionations in a Mn-rich anoxic marine sediment, Gullmar Fjord, Sweden. *Chemical Geology* **296-297**, 73-82.

Goldberg T., Gordon G., Izon G., Archer C., Pearce C. R., McManus J., Anbar A. D. and Rehkämper M. (2013) Resolution of inter-laboratory discrepancies in Mo isotope data: an intercalibration. *Journal of Analytical Atomic Spectrometry* **28**, 724-735

Goldberg T., Poulton S. W., Wagner T., Kolonic S. F. and Rehkämper M. (2016) Molybdenum drawdown during Cretaceous Oceanic Anoxic Event 2. *Earth and Planetary Science Letters* **440**, 81-91.

Goto K. T., Anbar A. D., Gordon G. W., Romaniello S. J., Shimoda G., Takaya Y. Tokumaru A., Nozaki T., Suzuki K., Machida S., Hanyu T. and Usui A. (2014) Uranium isotope systematics of ferromanganese crusts in the Pacific Ocean: Implications for the marine $^{238}U/^{235}U$ isotope system. *Geochimica et Cosmochimica Acta* **146**, 43-58.

Gray J. and Boucot A. J. (1979) The Devonian land plant *Protosalvinia*. *Lethaia* **12**, 57-63.

Hamblin A.P. (2010) Detailed outcrop and core measured sections of the Kettle Point formation, southwestern Ontario, with reference to shale gas potential, *Geological Survey of Canada*, Open File 6579.

Harris D. (1984) Graphic logs of oil shale intervals–Ordovician Collingwood Member and the Devonian Kettle Point and Marcellus formations. *Ontario Geological Survey*, Open File Report 5527.

Hayes J. M., Strauss H. and Kaufman A. J. (1999) The abundance of ^{13}C in marine organic matter and isotopic fractionation in the global biogeochemical cycle of carbon during the past 800 Ma. *Chemical Geology* **161**, 103-125.

Hein J. and Koschinsky A. (2014) Deep-ocean ferromanganese crusts and nodules. In: Scott S. D. (Ed.), Treatise on Geochemistry 2nd Edition, Volume 13, pp. 273-291.

Herrmann A. D., Kendall B., Algeo T. J., Gordon G. W., Wasylenki L. E. and Anbar A. D. (2012) Anomalous molybdenum isotope trends in Upper Pennsylvanian euxinic facies: Significance for use of $\delta^{98}Mo$ as a global marine redox proxy. *Chemical Geology* **324-325**, 87-98.

Holmden C., Amini M. and Francois R. (2015) Uranium isotope fractionation in Saanich Inlet: A modern analog study of a paleoredox tracer. *Geochimica et Cosmochimica Acta* **153**, 202-215.

Joachimski M. M. and Buggisch W. (1993) Anoxic events in the late Frasnian—Causes of the Frasnian-Famennian faunal crisis? *Geology* **21**, 675-678.

Johnson J. G., Klapper G. and Sandberg C. A. (1985) Devonian eustatic fluctuations in Euramerica. *Geological Society of America Bulletin* **96**, 567-587.

Johnson J. G., Klapper G. and Elrick M. (1996) Devonian transgressive–regressive cycles and biostratigraphy, northern Antelope Range, Nevada, establishment of reference horizons for global cycles. *Palaios* **11**, 3-14.

Kaltenbach A. (2013) Uranium isotopic analysis of terrestrial and extraterrestrial samples. PhD thesis, University of Otago.

Kendall B., Brennecka G. A., Weyer S. and Anbar A. D. (2013) Uranium isotope fractionation suggests oxidative uranium mobilization at 2.50 Ga. *Chemical Geol*ogy **362**, 105-114.

Kendall B., Creaser R. A., Gordon G. W. and Anbar A. D. (2009) Re–Os and Mo isotope systematics of black shales from the Middle Proterozoic Velkerri and Wollogorang Formations, McArthur Basin, northern Australia. *Geochimica et Cosmochimica Acta* **73**, 2534-2558.

Kendall B., Komiya T., Lyons T. W., Bates S. M., Gordon G. W., Romaniello S. J., Jiang G., Creaser R. A., Xiao S., McFadden K., Sawaki Y., Tahata M., Shu D., Han J., Li Y., Chu X. and Anbar A. D. (2015) Uranium and molybdenum isotope evidence for an episode of widespread ocean oxygenation during the late Ediacaran Period. *Geochimica et Cosmochimica Acta* **156**, 173-193.

Kendall B.*, Dahl T.W.* and Anbar A.D. (2017) Good golly, why moly? The stable isotope geochemistry of molybdenum. *Reviews in Mineralogy and Geochemistry* **82**, 683-732. *These authors contributed equally.

King E. K. and Pett-Ridge J. C. (2018) Reassessing the dissolved molybdenum isotopic composition of ocean inputs: the effect of chemical weathering and groundwater. *Geology* **46**, 955-958.

Klapper G. (1989) The Montagne Noire Frasnian (Upper Devonian) conodont succession. In: McMillan, N.J., Embry, A.E., Glass, D.J. (Eds.), Devonian of the World. Calgary, *Canadian Society of Petroleum Geologists Memoir* **14 (3)**, 449-468. [imprint 1988].

Klapper G. and Kirchgasser W. T. (2016) Frasnian Late Devonian conodont biostratigraphy in New York: graphic correlation and taxonomy. *Journal of Paleontology* **90**, 525-554.

Lu X., Kendall B., Stein H. J., Li C., Hannah J. L., Gordon G. W. and Ebbestad J. O. R. (2017) Marine redox conditions during deposition of Late Ordovician and Early Silurian organic-rich mudrocks in the Siljan ring district, central Sweden. *Chemical Geology* **457**, 75-94.

Lyons T. W. and Severmann S. (2006) A critical look at iron paleoredox proxies: new insights from modern euxinic marine basins. *Geochimica et Cosmochimica Acta* **70**, 5698-5722.

Lyons T. W., Werne J. P., Hollander D. J. and Murray R. W. (2003) Contrasting sulfur geochemistry and Fe/Al and Mo/Al ratios across the last oxic-to-anoxic transition in the Cariaco Basin, Venezuela. *Chemical Geology* **195**, 131-157.

Maynard J. B. (1991) Carbon isotopes as indicators of dispersal patterns in Devonian-Mississippian shales of the Appalachian Basin. *Geology* **9**, 262-265.

Meyer K. M. and Kump L. R. (2008) Oceanic euxinia in Earth history: causes and consequences. *Annual Reviews of Earth and Planetary Sciences* **36**, 251-288.

Miller C. A, Peucker-Ehrenbrink B., Walker B. D., and Marcantonio F. (2011) Re-assessing the surface cycling of molybdenum and rhenium. *Geochimica et Cosmochimica Acta* **75**, 7146-7179.

Montoya-Pino C., Weyer S., Anbar A. D., Pross J., Oschmann W., van de Schootbrugge B. and Arz H. W. (2010) Global enhancement of ocean anoxia during Oceanic Anoxic Event 2: A quantitative approach using U isotopes. *Geology* **38**, 315-318.

Morford J. L., Emerson S. R., Breckel E. J. and Kim S. H. (2005) Diagenesis of oxyanions (V, U, Re, and Mo) in pore waters and sediments from a continental margin. *Geochimica et Cosmochimica Acta* **69**, 5021-5032.

Nägler T. F., Neubert N., Böttcher M. E., Dellwig O. and Schnetger B. (2011) Molybdenum isotope fractionation in pelagic euxinia: Evidence from the modern Black and Baltic Seas. *Chemical Geology* **289**, 1-11.

Nägler T. F., Anbar A. D., Archer C., Goldberg T., Gordon G. W., Greber N. D., Siebert C., Sohrin Y. and Vance D. (2014) Proposal for an international molybdenum isotope measurement standard and data representation. *Geostandards and Geoanalytical Research* **38**, 149-151.

Nakagawa Y., Takano S., Firdaus M. L., Norisuye K., Hirata T., Vance D. and Sohrin Y. (2012). The molybdenum isotopic composition of the modern ocean. *Geochemical Journal* **46**, 131-141.

Neubert N., Nägler T. F. and Böttcher M. E. (2008) Sulfidity controls molybdenum isotope fractionation into euxinic sediments: Evidence from the modern Black Sea. *Geology* **36**, 775-778.

Noordmann J., Weyer S., Montoya-Pino C., Dellwig O., Neubert N., Eckert S., Paetzel M. and Böttcher M. E. (2015) Uranium and molybdenum isotope systematics in modern euxinic

basins: case studies from the central Baltic Sea and the Kyllaren fjord (Norway). *Chemical Geology* **396**, 182-195.

Noordmann J., Weyer S., Georg R. B., Jons S. and Sharma M. (2016) $^{238}U/^{235}U$ isotope ratios of crustal material, rivers and products of hydrothermal alteration: new insights on the oceanic U isotope mass balance. *Isotopes in Environmental and Health Studies* **52**, 141-163.

Obermajer M., Fowler M. G., Goodarzi F. and Snowdon L. R. (1997) Organic petrology and organic geochemistry of Devonian black shales in southwestern Ontario, Canada. *Organic Geochemistry* **26**, 229-246.

Ostrander C. M., Sahoo S. K., Kendall B., Jiang G., Planavsky N. J., Lyons T. W., Nielsen S. G., Owens J. D., Gordon G. W., Romaniello S. J. and Anbar A. D. (2019) Multiple negative molybdenum isotope excursions in the Doushantuo Formation (South China) fingerprint complex redox-related processes in the Ediacaran Nanhua Basin. *Geochimica et Cosmochimica Acta* 261, 191-209.

Over D. J., Lazar R., Baird G. C., Schieber J. and Ettensohn F. R. (2009) *Protosalvinia* Dawson and associated conodonts of the Upper *trachytera* Zone, Famennian, Upper Devonian, in the eastern United States. *Journal of Paleontology* **83**, 70-79.

Over D. J., Hauf E., Wallace J., Chiarello J., Over J.-S., Gilleaudeau G., Yi S. and Algeo T. (2019) Conodont biostratigraphy and magnetic susceptibility of Upper Devonian Chattanooga Shale, eastern United States: evidence for episodic deposition and disconformities. *Palaeogeography, Palaeoclimatology, Palaeoecology* **524**, 137-149.

Partin C. A., Bekker A., Planavsky N. J., Scott C. T., Gill B. C., Li C., Podkovyrov V., Maslov A., Konhauser K. O., Lalonde S. V., Love G. D., Poulton S. W. and Lyons T. W. (2013) Large-

scale fluctuations in Precambrian atmospheric and oceanic oxygen levels from the record of U in shales. *Earth and Planetary Science Letters* **369-370**, 284-293.

Pearce C. R., Cohen A. S., Coe A. L. and Burton K. W. (2008) Molybdenum isotope evidence for global ocean anoxia coupled with perturbations to the carbon cycle during the Early Jurassic. *Geology* **36**, 231-234.

Poulson Brucker R. L., McManus J., Severmann S. and Berelson W. M. (2009) Molybdenum behavior during early diagenesis: Insights from Mo isotopes. *Geochemistry, Geophysics, Geosystems* **10**, Q06010.

Poulson R. L., Siebert C., McManus J. and Berelson W. M. (2006) Authigenic molybdenum isotope signatures in marine sediments. *Geology* **34**, 617-620.

Poulton S. W. and Canfield D. E. (2005) Development of a sequential extraction procedure for iron: implications for iron partitioning in continentally derived particulates. *Chemical Geology* **214**, 209-221.

Poulton S. W. and Canfield D. E. (2011) Ferruginous conditions: a dominant feature of the ocean through Earth's history. *Elements* **7**, 107-112.

Quijada M., Riboulleau A., Strother P., Taylor W., Mezzetti A. and Versteegh G.J.M. (2016) *Protosalvinia* revisited, new evidence for a land plant affinity. *Review of Palaeobotany and Palynology* **227**, 52-64.

Raiswell R. and Berner R. A. (1985) Pyrite formation in euxinic and semi-euxinic sediments. *American Journal of Science* **285**, 710-724.

Raiswell R., Hardisty D. S., Lyons T. W., Canfield D. E., Owens J. D., Planavsky N. J., Poulton S. W. and Reinhard C. T. (2018) The iron paleoredox proxies: a guide to the pitfalls, problems and proper practice. *American Journal of Science* **318**, 491-526.

Reinhard C. T., Planavsky N. J., Robbins L. J., Partin C. A., Gill B. C., Lalonde S. V., Bekker A., Konhauser K.O. and Lyons T. W. (2013) Proterozoic ocean redox and biogeochemical stasis. *Proceedings of the National Academy of Sciences USA* **110**, 5357-5362.

Rolison J. M., Stirling C. H., Middag R. and Rijkenberg M. J. A. (2017) Uranium stable isotope fractionation in the Black Sea: modern calibration of the $^{238}U/^{235}U$ paleo-redox proxy. *Geochimica et Cosmochimica Acta* **203**, 69-88.

Romaniello S. J., Herrmann A. D. and Anbar A. D. (2013) Uranium concentrations and $^{238}U/^{235}U$ isotope ratios in modern carbonates from the Bahamas: Assessing a novel paleoredox proxy. *Chemical Geology* **362**, 305-316.

Rudnick R. L. and Gao S. (2003) Composition of the continental crust. *Treatise on Geochemistry 1st Edition*, Elsevier, volume 3, pp. 1-64.

Russell D. J. (1985) Depositional analysis of a black shale by using gamma-ray stratigraphy: The Upper Devonian Kettle Point formation of Ontario. *Bulletin of Canadian Petroleum Geology* **33**, 236-253.

Sanford B. V. and Brady W. B. (1955) Paleozoic geology of the Windsor-Sarnia area, Ontario. *Geological Survey of Canada Memoir 278.*

Schauble E. A. (2007) Role of nuclear volume in driving equilibrium stable isotope fractionation of mercury, thallium, and other very heavy elements. *Geochimica et Cosmochimica Acta* **71**, 2170-2189.

Schieber J. (2011) Marcasite in black shales – A mineral proxy for oxygenated bottom waters and intermittent oxidation of carbonaceous muds. *Journal of Sedimentary Research* **81**, 447–458.

Scholz F., McManus J. and Sommer S. (2013) The manganese and iron shuttle in a modern euxinic basin and implications for molybdenum cycling at euxinic ocean margins. *Chemical Geology* **355**, 56-68.

Scholz F., Baum M., Siebert C., Eroglu S., Dale A. W., Naumann M., and Sommer S. (2018) Sedimentary molybdenum cycling in the aftermath of seawater inflow to the intermittently euxinic Gotland Deep, central Baltic Sea. *Chemical Geology* **491**, 27-38.

Scott C., Lyons T. W., Bekker A., Shen Y., Poulton S. W., Chu X. and Anbar A. D. (2008) Tracing the stepwise oxygenation of the Proterozoic ocean. *Nature* **452**, 456-459.

Scott C., Slack J. F. and Kelley K. D. (2017) The hyper-enrichment of V and Zn in black shales of the Late Devonian-Early Mississippian Bakken Formation (USA). *Chemical Geology* **452**, 24-33.

Siebert C., Nägler T. F., von Blanckenburg F. and Kramers J. D. (2003) Molybdenum isotope records as a potential new proxy for paleoceanography. *Earth and Planetary Science Letters* **211**, 159-171.

Siebert C., McManus J., Bice A., Poulson R. and Berelson W. M. (2006) Molybdenum isotope signatures in continental margin sediments. *Earth and Planetary Science Letters* **241**, 723-733.

Skei J., Loring D. H. and Rantala R. T. T. (1988) Partitioning and enrichment of trace metals in a sediment core from Framvaren, south Norway. *Marine Chemistry* **23**, 269-281.

Snowdon L. R. (1984) A comparison of RockEval pyrolysis and solvent extract results from the Collingwood and Kettle Point oil shales, Ontario. *Bulletin of Canadian Petroleum Geology* **32**, 327-334.

Song H., Song H., Algeo T. J., Tong J., Romaniello S. J., Zhu Y., Chu D., Gong Y. and Anbar A. D. (2017) Uranium and carbon isotopes document global-ocean redox-productivity relationships linked to cooling during the Frasnian-Famennian mass extinction. *Geology* **45**, 887-890.

Spalletta C., Perri M. C., Over D. J. and Corradini C. (2017) Famennian (Upper Devonian) conodont zonation: revised global standard. *Bulletin of Geosciences* **92**, 31-57.

Stirling C. H., Andersen M. B., Potter E. K. and Halliday A. N. (2007) Low-temperature isotopic fractionation of uranium. *Earth and Planetary Science Letters* **264**, 208-225.

Stirling C. H., Andersen M. B., Warthmann R. and Halliday A. N. (2015) Isotope fractionation of ^{238}U and ^{235}U during biologically-mediated uranium reduction. *Geochimica et Cosmochimica Acta* **163**, 200-218.

Stylo M., Neubert N., Wang Y., Monga N., Romaniello S. J., Weyer S. and Bernier-Latmani R. (2015) Uranium isotopes fingerprint biotic reduction. *Proceedings of the National Academy of Sciences* **112**, 5619-5624.

Tissot F. L. and Dauphas N. (2015) Uranium isotopic compositions of the crust and ocean: Age corrections, U budget and global extent of modern anoxia. *Geochimica et Cosmochimica Acta* **167**, 113-143.

Tissot F. L. H., Chen C., Go B. M., Naziemiec M., Healy G., Bekker A., Swart P. K. and Dauphas N. (2018) Controls on eustasy and diagenesis on the $^{238}U/^{235}U$ of carbonates and evolution of the seawater ($^{234}U/^{238}U$) during the last 1.4 Myr. *Geochimica et Cosmochimica Acta* **242**, 233-265.

Tribovillard N., Algeo T. J., Lyons T. and Riboulleau A. (2006) Trace metals as paleoredox and paleoproductivity proxies: an update. *Chemical Geology* **232**, 12-32.

Tossell J. A. (2005) Calculating the partitioning of the isotopes of Mo between oxidic and sulfidic species in aqueous solution. *Geochimica et Cosmochimica Acta* **69**, 2981-2993.

Voegelin A. R., Pettke T., Greber N.D., von Niederhäusern B. and Nägler T. F. (2014) Magma differentiation fractionates Mo isotope ratios: evidence from the Kos Plateau Tuff (Aegean Arc). *Lithos* **190**, 440-448.

Wang X., Johnson C. M. and Lundstrom C. C. (2015) Isotope fractionation during oxidation of tetravalent U by dissolved oxygen. *Geochimica et Cosmochimica Acta* **150**, 160-170.

Wang X., Planavsky N. J., Reinhard C. T., Hein J. R. and Johnson T. M. (2016) A Cenozoic seawater redox record derived from $^{238}U/^{235}U$ in ferromanganese crusts. *American Journal of Science* **316**, 64-83.

Wasylenki L. E., Rolfe B. A., Weeks C. L., Spiro T. G. and Anbar A. D. (2008) Experimental investigation of the effects of temperature and ionic strength on Mo isotope fractionation during adsorption to manganese oxides. *Geochimica et Cosmochimica Acta* **72**, 5997-6005.

Wei W. and Algeo T. J. (in press) Elemental proxies for paleosalinity analysis of ancient shales and mudrocks. *Geochimica et Cosmochimica Acta*. DOI: https://doi.org/10.1016/j.gca.2019.06.034.

Wei W., Algeo T. J., Lu Y., Lu Y., Liu H., Zhang S., Peng L., Zhang J. and Chen L. (2018) Identifying marine incursions into the Paleogene Bohai Bay Basin lake system in northeastern China. *International Journal of Coal Geology* **200**, 1-17.

Westermann S., Vance D., Cameron V., Archer C. and Robinson S. A. (2014) Heterogeneous oxygenation states in the Atlantic and Tethys oceans during Oceanic Anoxic Event 2. *Earth and Planetary Science Letters* **404**, 178-189.

Weyer S., Anbar A. D., Gerdes A., Gordon G. W., Algeo T. J. and Boyle E. A. (2008) Natural fractionation of $^{238}U/^{235}U$. *Geochimica et Cosmochimica Acta* **72**, 345-359.

White D. A., Elrick M., Romaniello S. and Zhang F. (2018) Global seawater redox trends during the Late Devonian mass extinction detected using U isotopes of marine limestones. *Earth and Planetary Science Letters* **503**, 68-77.

Willbold M. and Elliott T. (2017) Molybdenum isotope variations in magmatic rocks. *Chemical Geology* **449**, 253-268.

Winder C. G. (1966) Conodont zones and stratigraphic variability in Upper Devonian rocks, Ontario. *Journal of Paleontology* **40**, 1275-1293.

Yang S., Kendall B., Lu X., Zhang F. and Zheng W. (2017) Uranium isotope compositions of mid-Proterozoic black shales: evidence for an episode of increased ocean oxygenation at 1.36 Ga and evaluation of the effect of post-depositional hydrothermal fluid flow. *Precambrian Research* **298**, 187-201.

Zhang F., Xiao S., Kendall B., Romaniello S. J., Cui H., Meyer M., Gilleaudeau G. J., Kaufman A. J. and Anbar A. D. (2018) Extensive marine anoxia during the terminal Ediacaran Period. *Science Advances* **4**, eaan8993.

Figure Captions

Figure 1. Geological map showing the location of the Chatham Sag in which the Kettle Point Formation was deposited. Also shown is the 'Gore of Chatham' (GoC) core from which samples were obtained for this study. The Chatham Sag links the Michigan and Appalachian basins. Modified from Bingham-Koslowski et al. (2016) and Armstrong and Carter (2010).

Figure 2. Comparison of metal concentrations and total organic carbon contents of the Kettle Point black shales for **A)** molybdenum, **B)** uranium, and **C)** vanadium.

Figure 3. Comparison of metal concentrations and total sulfur contents of the Kettle Point black shales for **A)** molybdenum, **B)** uranium, and **C)** vanadium.

Figure 4. Lithostratigraphic and geochemical profiles (redox-sensitive elemental data and Mo, U, and organic C isotope data from black shales; no data are reported for the grey-green mudstones) through the Kettle Point Formation in the Gore of Chatham core. In the lithostratigraphic profile, Units 1 and 3 contain interlaminated black shale interbedded with grey-green mudstone (tan shading) as well as thicker intervals of grey-green mudstone with rare or negligible black shale beds (green shading) and black shale with rare or negligible grey-green mudstone beds (black shading). Units 2 and 4 are dominated by non-interlaminated black shale (black shading). In the Mo and U isotope profiles, open squares denote bulk sample isotope compositions and filled circles denote authigenic isotope compositions. The horizontal dashed line denotes the Frasnian-Famennian boundary based on conodont biostratigraphy. EF = Al-normalized enrichment factor; TOC = total organic carbon; TS = total sulfur.

Figure 5. Lithostratigraphic and geochemical profiles (paleosalinity elemental data and Mo and U isotope data from black shales; no data are reported for the grey-green mudstones) through the Kettle Point Formation in the Gore of Chatham core. In the lithostratigraphic profile, Units 1 and 3 contain interlaminated black shale interbedded with grey-green mudstone (tan shading) as well

as thicker intervals of grey-green mudstone with rare or negligible black shale beds (green shading) and black shale with rare or negligible grey-green mudstone beds (black shading). Units 2 and 4 are dominated by non-interlaminated black shale (black shading). Salinity thresholds for the B/Ga, Sr/Ba, and TS/TOC ratios are after Wei and Algeo (in press). In the Mo and U isotope profiles, open squares denote bulk sample isotope compositions and filled circles denote authigenic isotope compositions. The horizontal dashed line denotes the Frasnian-Famennian boundary based on conodont biostratigraphy. TOC = total organic carbon; TS = total sulfur.

Figure 6. Crossplots of **A)** bulk δ^{98}Mo versus δ^{238}U, and **B)** authigenic δ^{98}Mo versus δ^{238}U, showing a strong inverse correlation between the Mo and U isotope compositions of the Kettle Point black shales.

Figure 7. Crossplots of **A)** bulk δ^{98}Mo versus Mo EFs (enrichment factors), and **B)** bulk δ^{238}U versus U EFs of the Kettle Point black shales, showing minimal correlation in both cases.

Figure 8. Comparison of **A)** Fe versus TS (total sulfur) contents, **B)** Fe versus Al contents, and **C)** TS versus TOC (total organic carbon) contents of the Kettle Point black shales. For comparison, the pyrite Fe/S ratio is shown in A). A Fe/Al ratio is shown in B) to denote a possible maximum detrital Fe/Al ratio (see text for discussion).

Figure 9. Cross-plot of Mo versus U enrichment factors (EF) for the Kettle Point black shales, showing a strong positive correlation. The dashed lines are weight equivalents of the molar Mo/U ratio of modern seawater (1×SW and 3×SW) (after Algeo and Tribovillard, 2009).

Figure 10. Crossplots of **A)** authigenic δ^{98}Mo versus Sr/Ba ratios, **B)** authigenic δ^{238}U versus Sr/Ba ratios, **C)** authigenic δ^{98}Mo versus TS/TOC ratios, **D)** authigenic δ^{238}U versus TS/TOC ratios, **E)** authigenic δ^{98}Mo versus B/Ga ratios, and **F)** authigenic δ^{238}U versus B/Ga ratios of the Kettle Point black shales. The strongest statistically significant correlations occur between the isotope compositions and the B/Ga paleosalinity proxy.

Figure 11. Comparison of **A)** bulk δ^{98}Mo versus V enrichment factors (EFs) and **B)** Mo versus V EFs for the Kettle Point black shales. Open circles = Black shales above 57 m depth (upper Unit 4); filled circles = black shales below 57 m depth (Unit 1 to lower Unit 4).

Figure 12. Cross-plot of authigenic δ^{98}Mo versus δ^{238}U for the Kettle Point black shales, showing the similarity in slope with the trend defined by the mean values of most modern euxinic basins (S = Saanich Inlet, C = Cariaco Basin, B = Black Sea, K = Kyllaren Fjord, L = Lake Rogoznica; Bura-Nakić et al., 2018). The highly restricted Black Sea with its unusually long deep-water renewal time is the main exception to the modern trend and reflects a higher rate of Mo burial in sediments relative to U (which may cause the authigenic Mo and U isotope compositions of euxinic sediments to evolve along the trend from S through B) compared to other modern euxinic basins. The Kettle Point trend is offset to slightly lower isotopic compositions than the modern trend, suggesting that global seawater δ^{98}Mo and δ^{238}U during the Famennian (F-F SW) was slightly lower than modern seawater (MSW). The arrows depict the expected correlation between δ^{98}Mo and δ^{238}U if the main control on the stratigraphic isotopic trends in a euxinic black shale unit was

global ocean redox variations (positive) or changes in the local depositional environment (negative).

Figure 1

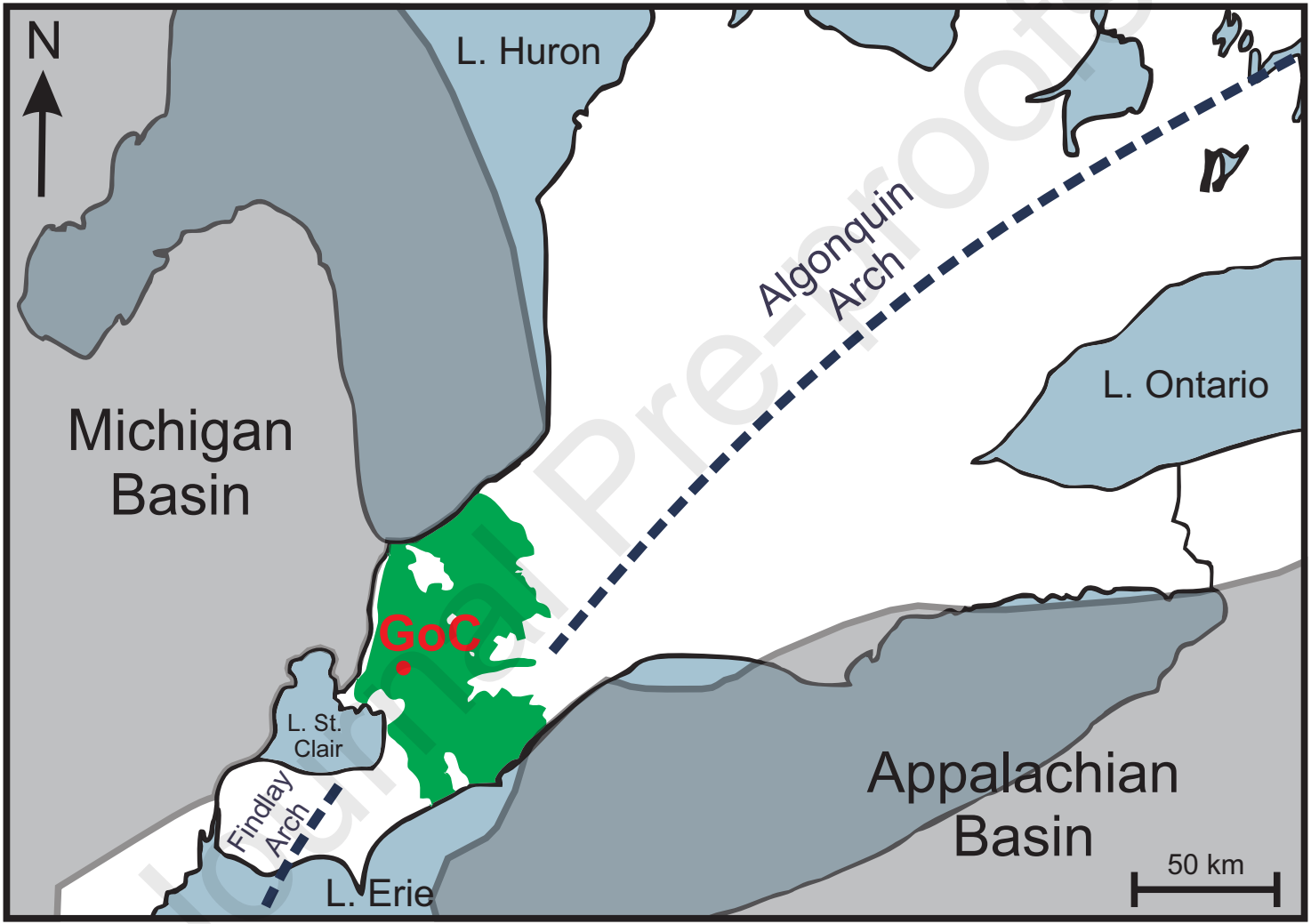

Figure 2

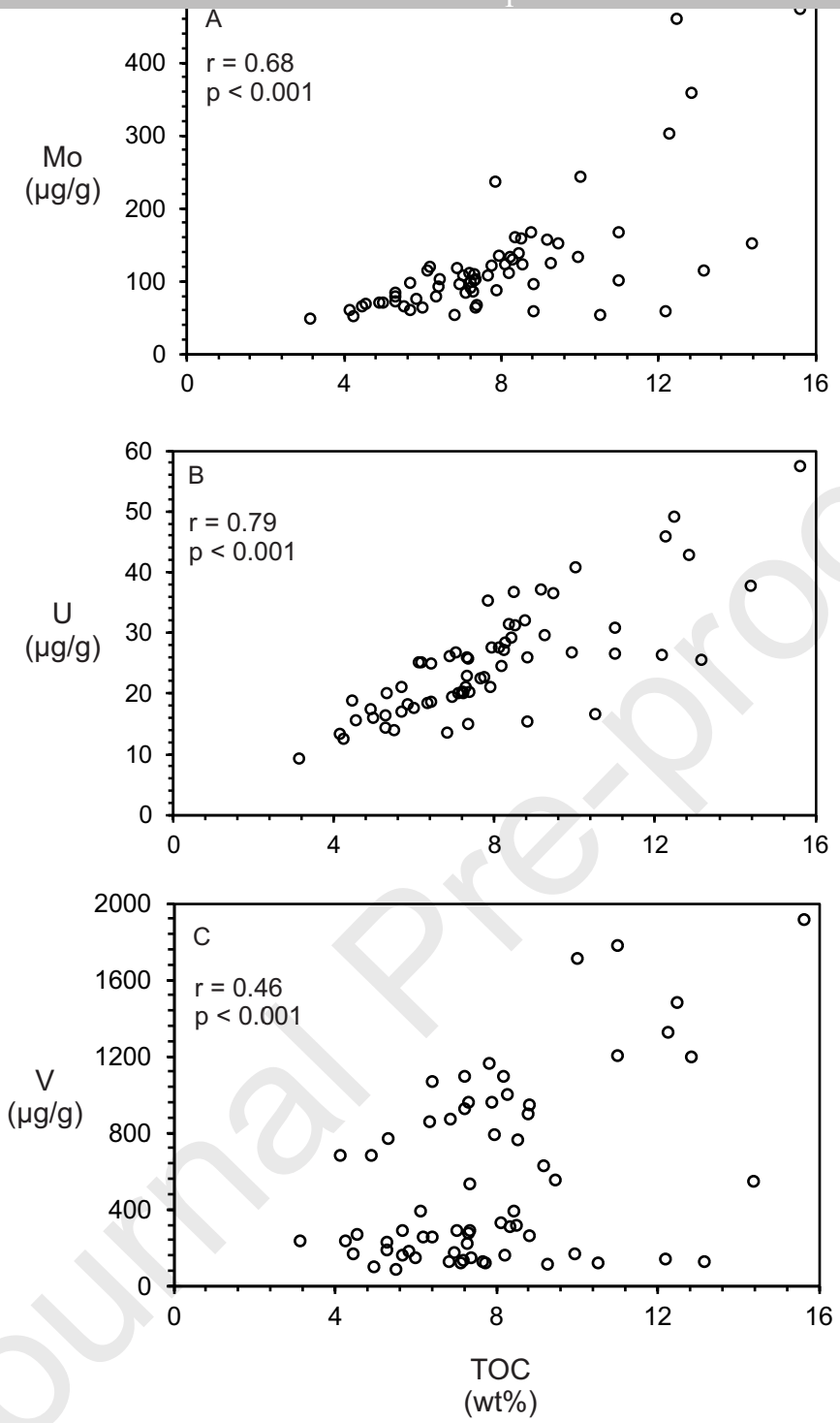

Figure 3

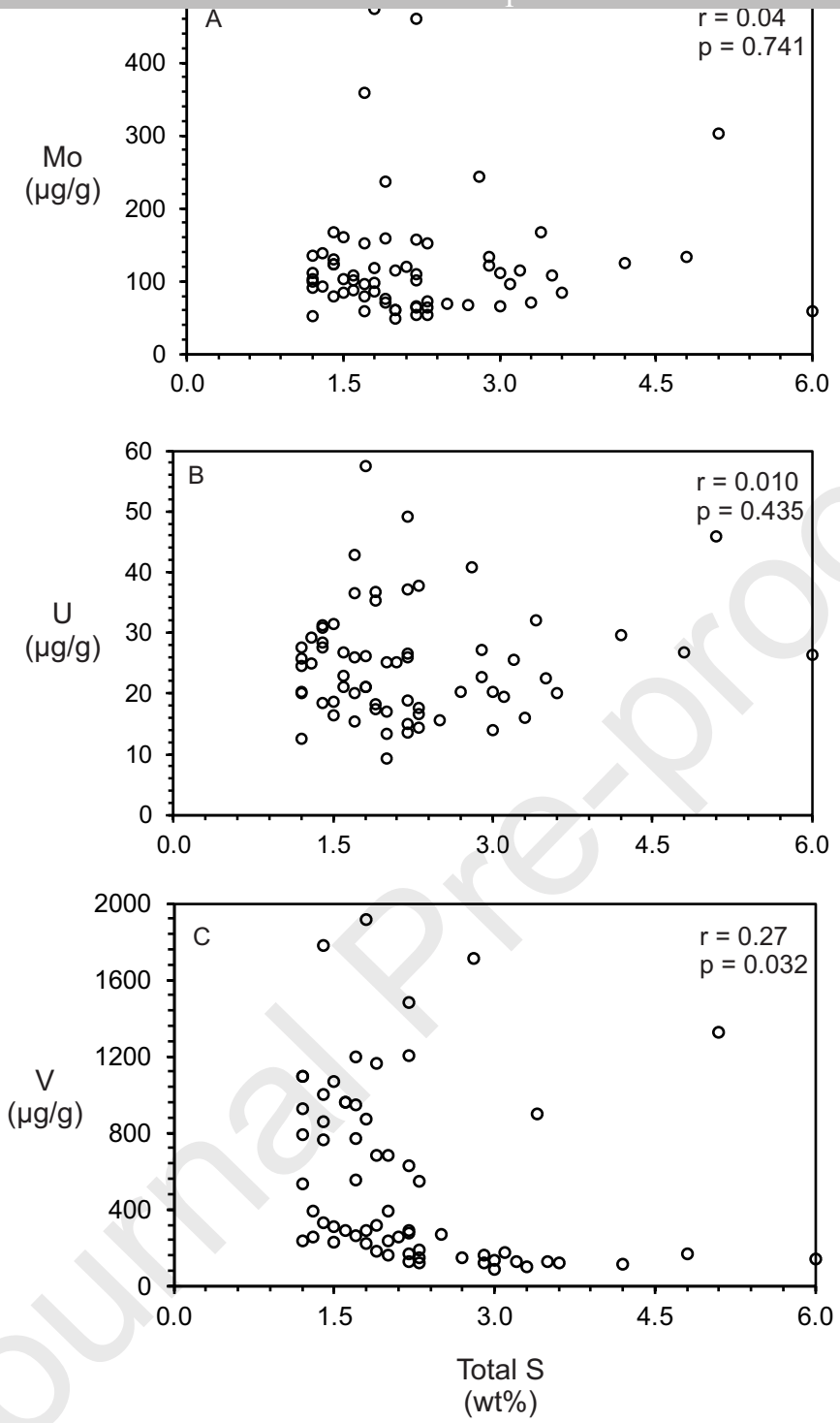

Figure 4

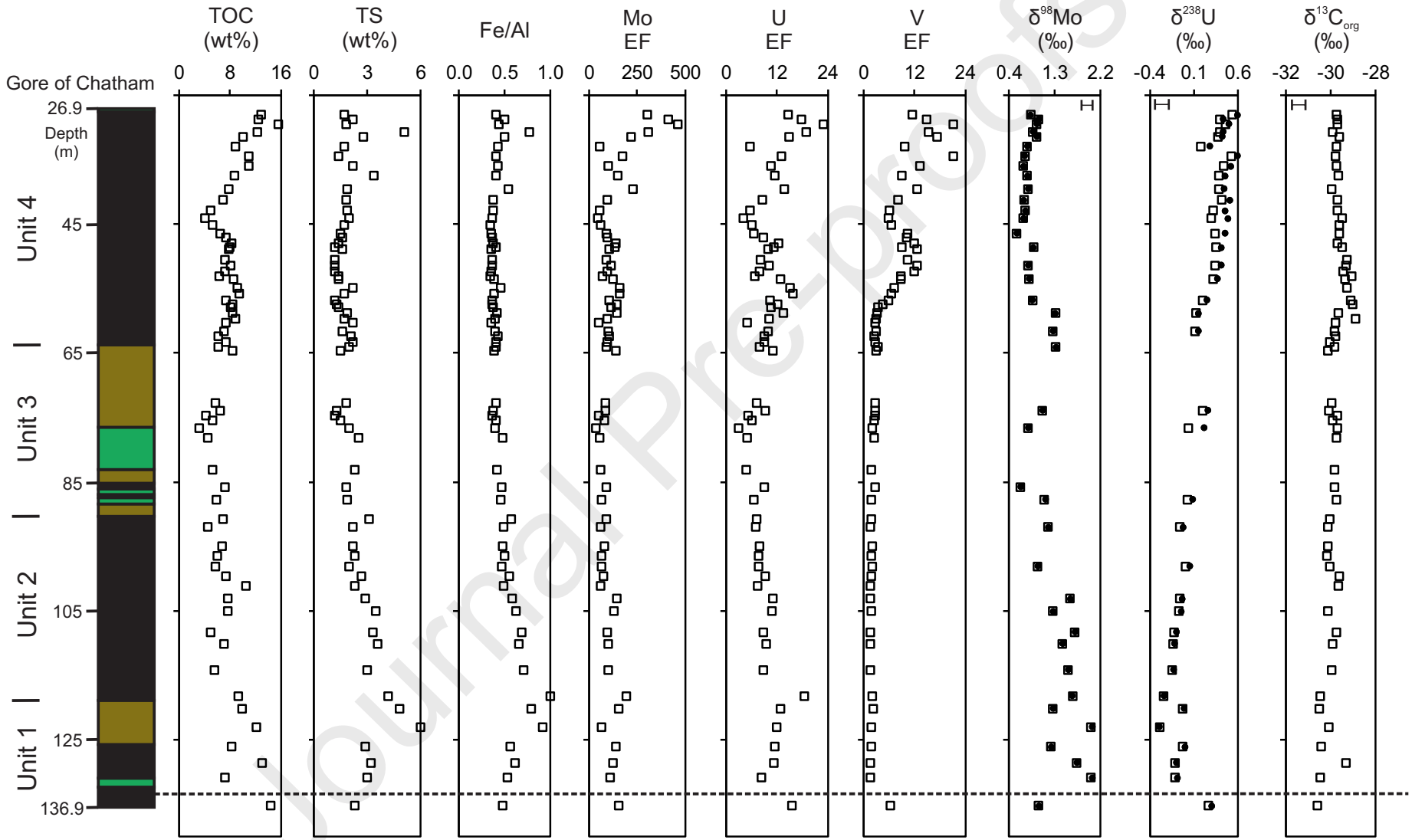

Figure 5

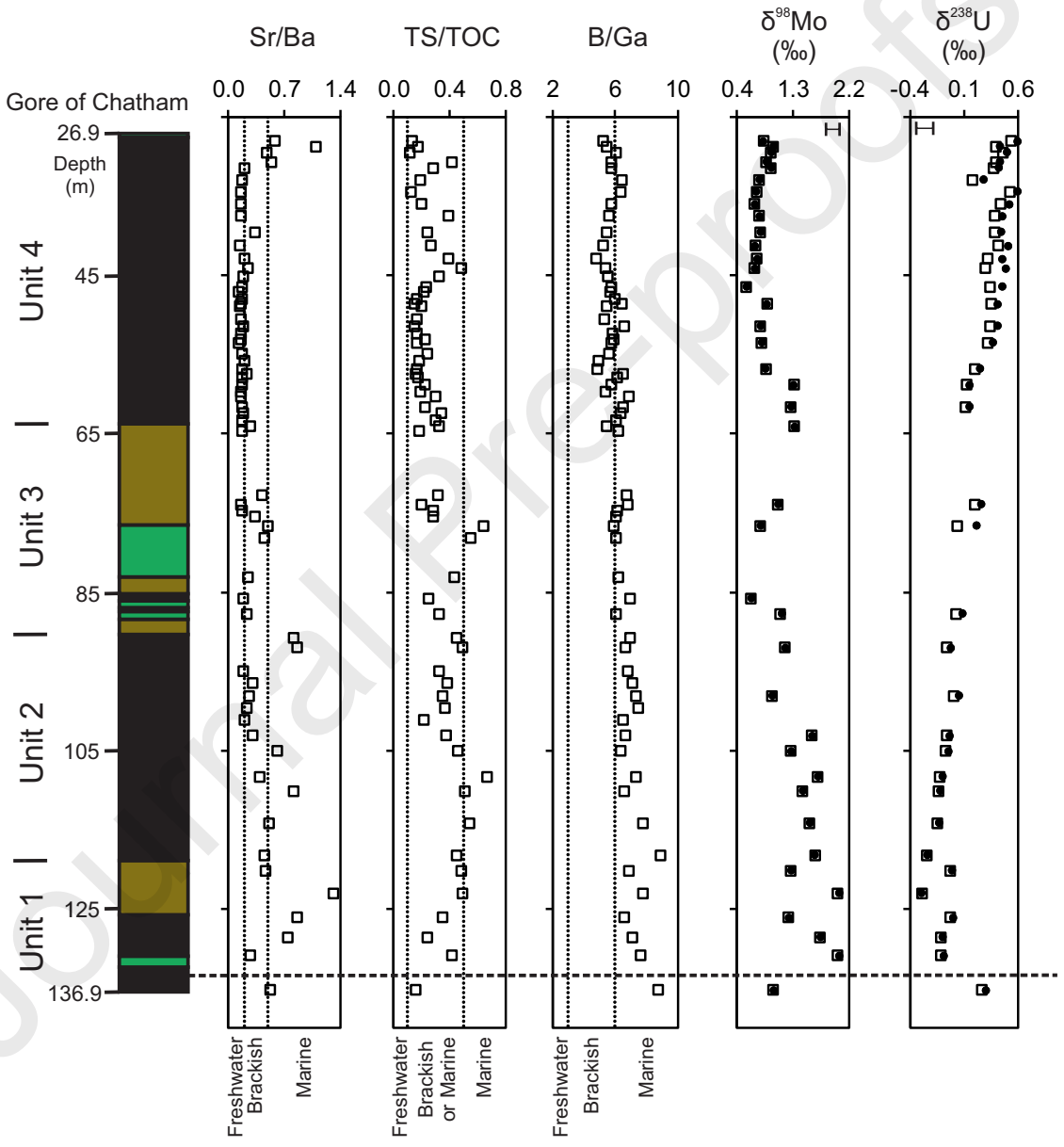

Figure 6

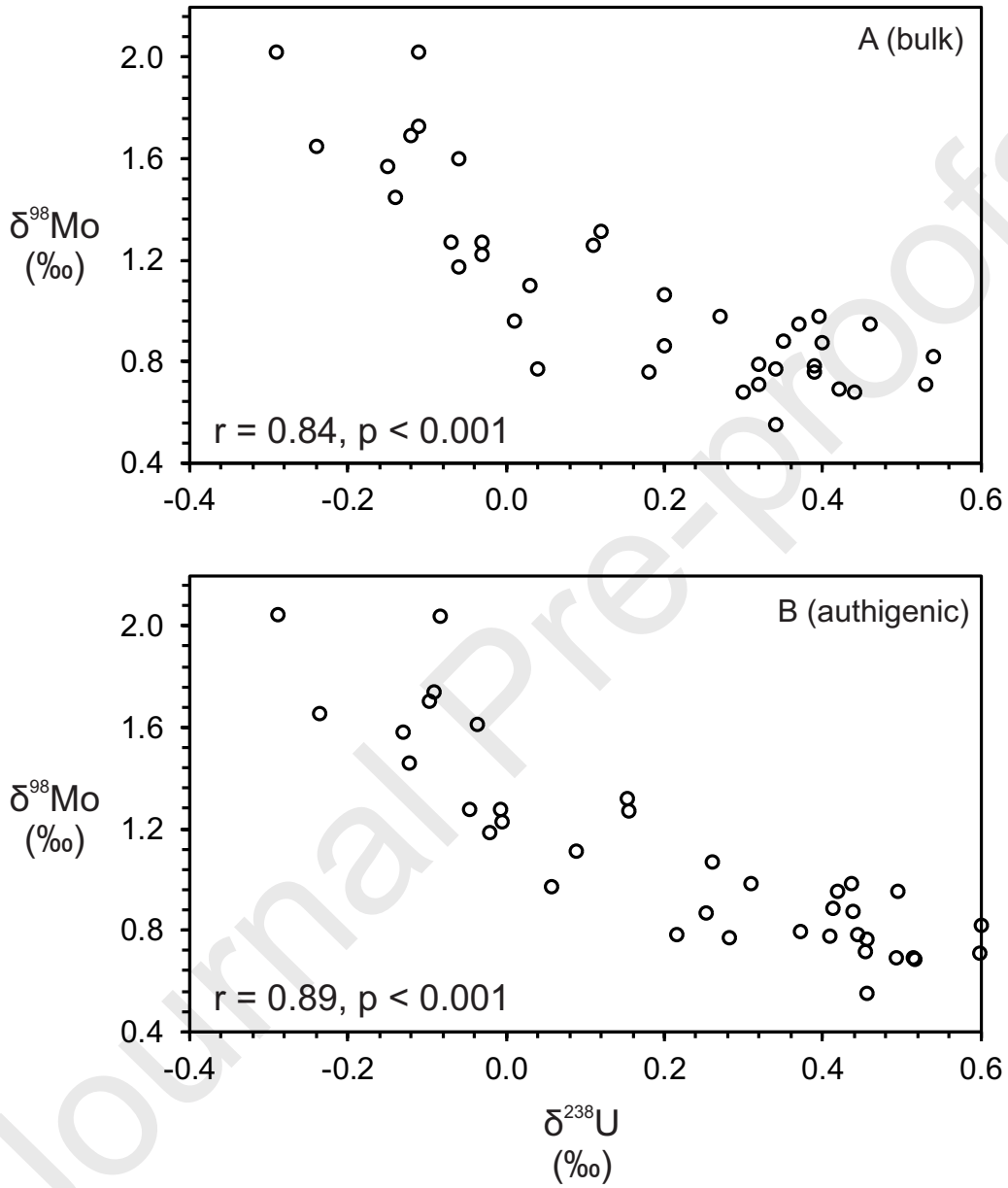

Figure 7

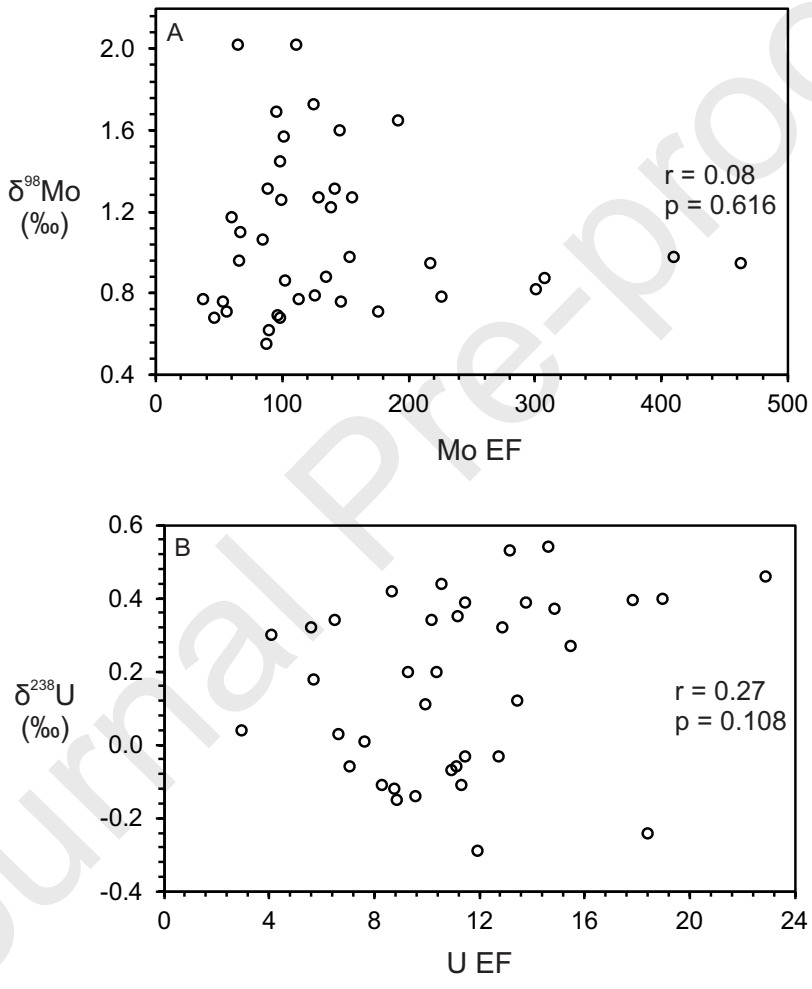

Figure 8

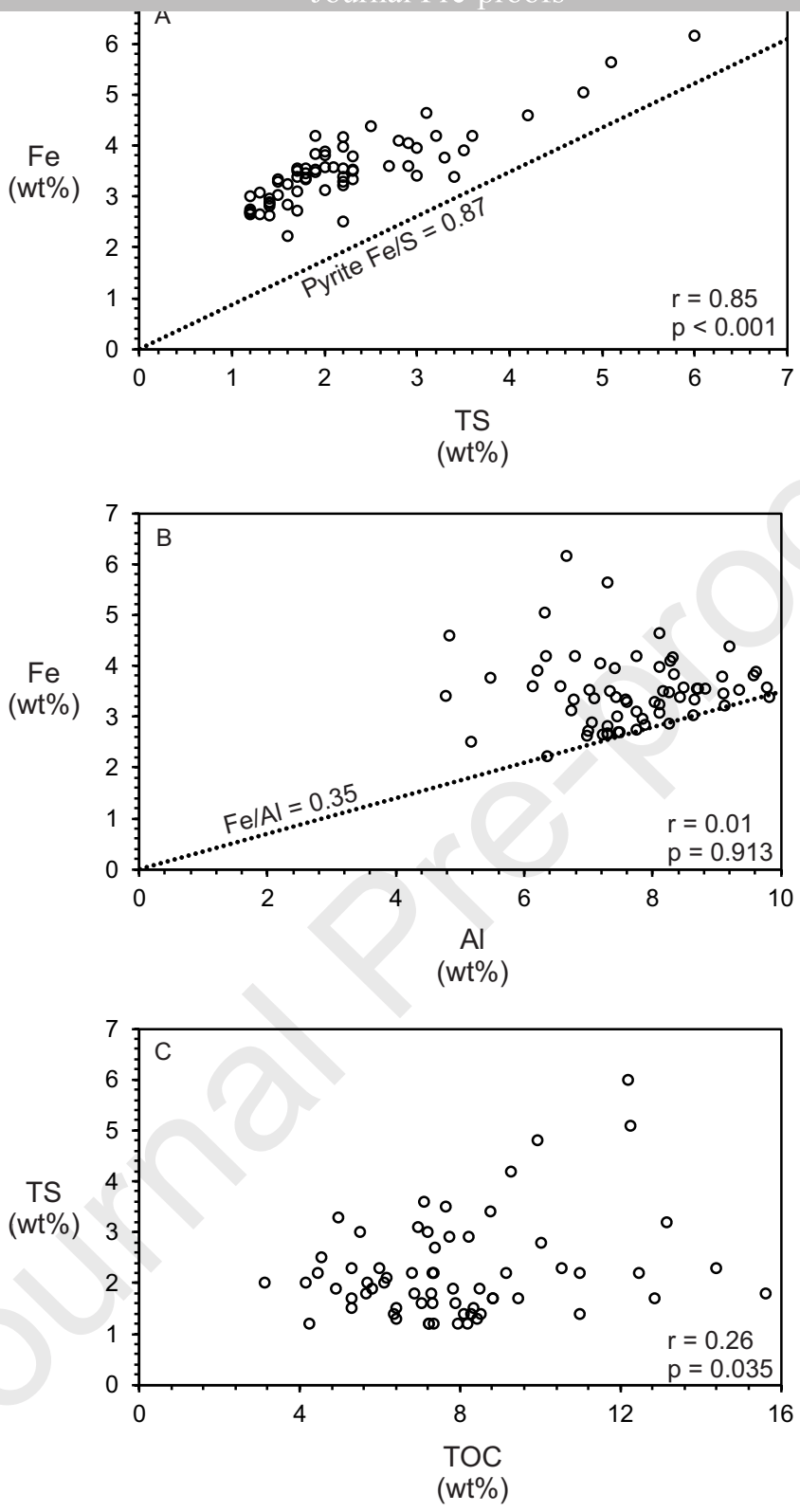

Figure 9

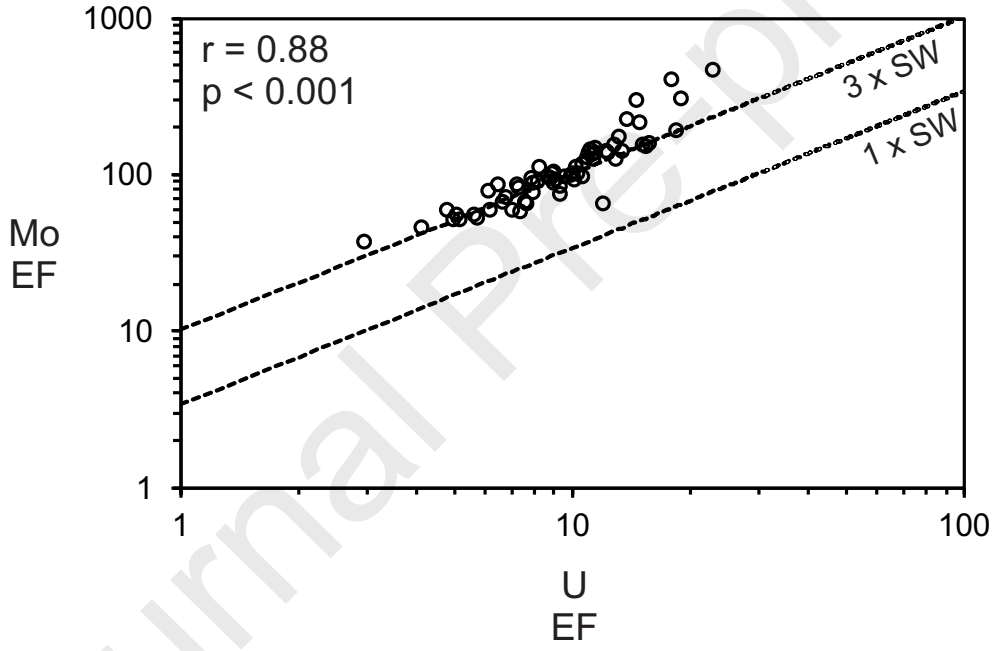

Figure 10

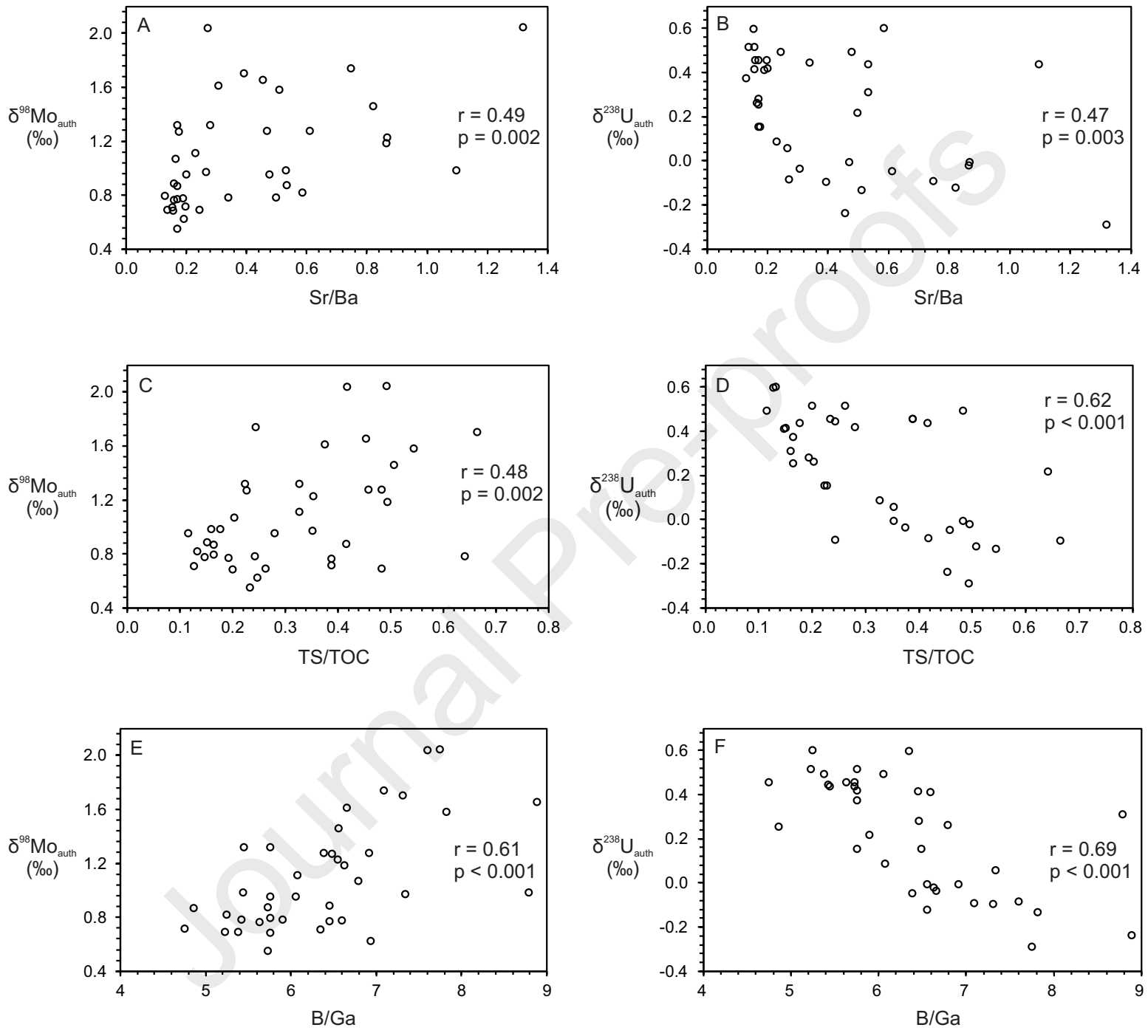

Figure 11

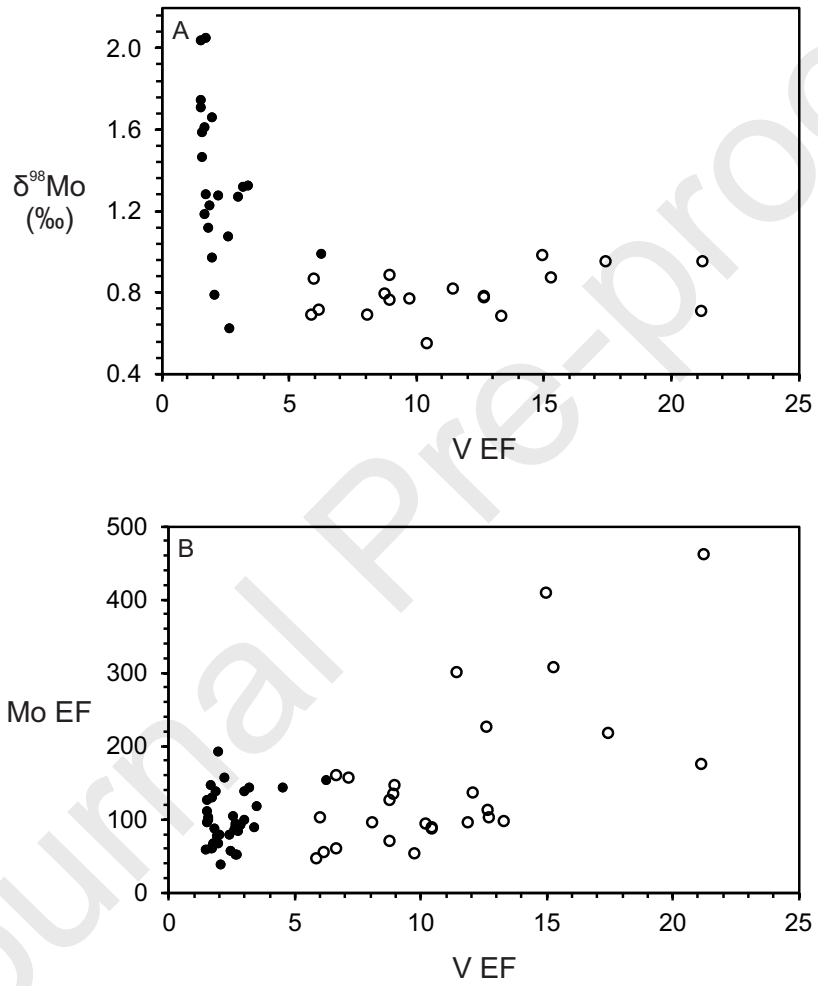

Figure 12

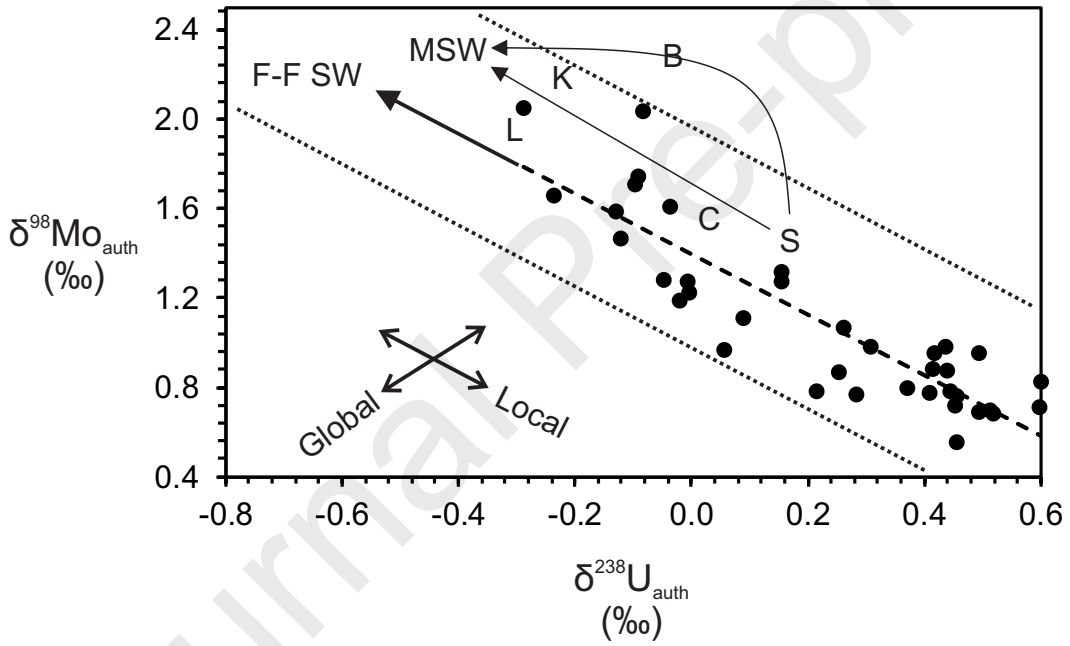

Table 1

Table 1. Elemental and organic carbon isotope data for black shales of the Kettle Point Formation

Sample	Height (m)	TIC (wt%)	TOC[a] (wt%)	TS[b] (wt%)	C	Ca (wt%)	Mg (wt%)	Fe (wt%)	Al (wt%)	Fe/Al	Sr (µg/g)	Ba (µg/g)	Sr/Ba	B (µg/g)	Ga (µg/g)	B/Ga	Mo (µg/g)	U (µg/g)	V (µg/g)	Mo[c] (EF)	U[c] (EF)	V[c] (EF)	Mo/TOC x 10^{-4}	$\delta^{13}C_{org}$ (‰)
Unit 4																								
KPZ-1	28.0	1.4	13	1.7	0.13	0.56	0.93	3.6	8.8	0.40	126	215	0.58	104	20	5.2	358	43	1198	300	15	11	28	-29.7
KPZ-2	28.7	1.6	12	2.2	0.18	0.63	1.0	4.2	8.3	0.50	94	86	1.1	107	20	5.4	459	49	1479	409	18	15	37	-29.7
KPZ-3	29.4	1.4	16	1.8	0.12	0.29	0.79	3.3	7.6	0.44	114	239	0.48	106	18	6.1	473	57	1912	463	23	21	30	-29.7
KPZ-4	30.6	1.1	12	5.1	0.42	0.14	0.77	5.6	7.3	0.77	64	120	0.53	103	18	5.7	302	46	1327	307	19	15	25	-29.9
KPZ-5	31.4	1.1	10	2.8	0.28	0.13	0.77	4.1	8.3	0.50	74	371	0.20	104	18	5.8	243	41	1715	217	15	17	24	-29.6
KPZ-6	32.9	0.86	8.8	1.7	0.19	0.29	0.92	3.5	8.2	0.43	67	394	0.17	123	19	6.5	59	15	945	53	5.7	9.7	6.6	-29.7
KPZ-7	34.4	1.3	11	1.4	0.13	0.22	0.76	2.9	7.1	0.41	61	393	0.15	103	16	6.3	168	31	1778	176	13	21	15	-29.8
KPW6	36.0	0.79	11	2.2	0.20	0.16	0.67	3.3	7.6	0.43	64	413	0.16	99	17	5.8	101	27	1204	98	11	13	9.2	-29.8
KPW4	37.5	1.1	8.8	3.4	0.39	0.27	0.72	3.4	8.4	0.40	78	491	0.16	110	19	5.6	167	32	897	147	11	9.0	19	-29.7
KPW5	39.5	0.89	7.8	1.9	0.24	0.56	0.73	4.2	7.8	0.54	72	213	0.34	101	19	5.4	236	35	1164	226	14	13	30	-29.9
KPW3	41.2	0.62	6.9	1.8	0.26	0.22	0.75	3.5	9.1	0.38	69	502	0.14	109	21	5.2	119	26	872	97	8.7	8.0	17	-29.7
KPW2	42.9	0.26	4.9	1.9	0.39	0.19	0.73	3.5	9.3	0.38	80	407	0.20	113	24	4.8	71	17	684	56	5.6	6.1	14	-29.7
KPW1	44.1	0.27	4.1	2.0	0.48	0.22	0.71	3.6	9.8	0.37	79	323	0.24	128	24	5.4	61	13	682	46	4.1	5.9	15	-29.5
KPR1	45.1	0.37	5.3	1.7	0.32	0.18	0.77	3.4	9.8	0.35	78	433	0.18	113	21	5.5	80	20	774	60	6.2	6.6	15	-29.6
KPR2	46.4	0.61	6.4	1.5	0.23	0.41	0.78	3.0	8.6	0.35	74	439	0.17	118	21	5.7	102	19	1071	88	6.5	10	16	-29.6
KPR3	47.1	0.73	7.3	1.6	0.22	0.18	0.73	2.8	7.9	0.36	68	529	0.13	106	19	5.7	101	23	957	95	8.8	10	14	
KPR4	47.9	1.1	8.3	1.4	0.17	0.66	0.74	2.6	7.0	0.38	68	399	0.17	113	19	6.0	130	28	1001	137	12	12	16	-29.7
KPR6	48.6	0.78	7.9	1.2	0.15	0.34	0.72	3.0	7.4	0.40	68	429	0.16	107	17	6.5	135	28	790	135	11	8.9	17	-29.5
KPR5	48.8	1.0	7.9	1.6	0.20	0.30	0.63	2.2	6.4	0.35	57	379	0.15	79	14	5.5	88	21	962	102	10	13	11	
KPR7	50.5	0.52	7.2	1.2	0.17	0.17	0.71	2.7	7.5	0.36	63	410	0.15	89	17	5.3	91	20	926	90	8.2	10	13	-29.3
KPR8	51.4	1.2	8.2	1.2	0.15	1.1	0.73	2.7	7.3	0.36	66	347	0.19	106	16	6.6	111	25	1097	113	10	13	14	-29.3
KPR9	52.3	0.82	7.2	1.2	0.17	0.18	0.71	2.7	7.7	0.35	62	393	0.16	105	18	5.9	100	20	1094	96	7.8	12	14	-29.5
KPR10	53.1	0.71	6.3	1.4	0.22	0.17	0.73	2.9	8.3	0.35	66	431	0.15	108	18	5.9	80	18	860	72	6.8	8.7	13	-29.1
KPR11	53.5	1.0	8.5	1.4	0.16	0.20	0.71	2.8	7.3	0.38	64	488	0.13	108	19	5.8	124	31	761	126	13	8.8	15	-29.4
KPR12	54.8	1.1	9.2	2.2	0.24	0.51	0.71	3.4	7.4	0.45	66	377	0.18	87	15	5.6	157	37	631	157	15	7.1	17	-29.3
KPR13	55.8	1.6	9.5	1.7	0.18	1.5	0.70	2.7	7.0	0.39	69	343	0.20	80	16	4.9	152	36	551	161	16	6.6	16	
KPR14	56.8	1.0	7.3	1.2	0.16	0.27	0.71	2.7	7.5	0.36	64	377	0.17	87	18	4.9	103	26	532	102	10	6.0	14	-29.1
KPR15	57.4	1.0	8.4	1.3	0.15	0.25	0.70	2.7	7.2	0.37	62	268	0.23	119	18	6.5	139	29	391	142	12	4.6	16	-29.0
KPR16	57.9	0.90	8.1	1.4	0.17	0.30	0.75	3.0	7.8	0.38	65	391	0.17	112	18	6.1	123	27	327	117	11	3.5	15	
KPR17	58.8	1.0	8.5	1.9	0.22	0.26	0.77	3.5	8.3	0.42	68	402	0.17	118	20	5.8	158	37	314	142	13	3.2	19	-29.7
KPR18	59.7	1.2	8.8	1.7	0.19	0.47	0.73	3.1	7.8	0.40	69	420	0.16	91	17	5.4	96	26	262	92	10	2.8	11	-28.9
KPP2	60.2	0.24	7.3	2.2	0.30	0.27	0.87	3.2	9.1	0.35	71	435	0.16	149	22	6.9	64	15	290	52	5.0	2.7	8.7	-29.8
KPP11	61.6	0.60	7.0	1.6	0.23	0.46	0.75	3.2	8.1	0.40	71	401	0.18	128	20	6.5	108	27	288	99	10	3.0	15	-29.8
KPP6	62.3	0.45	6.2	2.1	0.34	0.24	0.75	3.6	8.5	0.42	74	386	0.19	129	20	6.4	119	25	258	104	9.0	2.6	19	-29.8
KPP1	63.2	0.24	7.3	2.2	0.30	0.22	0.77	3.6	8.7	0.41	70	412	0.17	120	20	6.1	110	26	277	94	9.0	2.7	15	-30.1
KPP8	64.1	0.43	6.1	2.0	0.33	0.24	0.83	3.9	9.6	0.40	85	304	0.28	139	25	5.4	115	25	389	89	7.9	3.4	19	-29.8
KPP9	64.6	0.66	8.4	1.5	0.18	0.19	0.83	3.3	8.7	0.39	74	430	0.17	136	22	6.2	161	31	308	138	11	3.0	19	-30.1
Unit 3																								
KPP5	72.7	0.20	5.7	1.8	0.32	0.20	0.82	3.6	8.7	0.41	72	171	0.42	140	21	6.8	97	21	286	83	7.3	2.8	17	-30.0
KPP4	73.9	0.37	6.4	1.3	0.20	0.55	0.88	3.1	8.1	0.38	66	402	0.16	133	20	6.8	93	25	255	85	9.3	2.6	14	-30.1
KPP12	74.7	0.31	4.2	1.2	0.28	0.21	0.70	2.7	7.3	0.37	59	358	0.17	153	25	6.1	51	12	236	52	5.2	2.7	12	-29.7
KPP10	75.4	0.49	5.3	1.5	0.28	0.38	0.79	3.3	8.0	0.41	70	212	0.33	128	21	6.1	85	16	231	78	6.1	2.4	16	-29.9
KPP3	76.6	0.07	3.1	2.0	0.64	0.17	0.87	3.8	9.6	0.40	81	162	0.50	151	26	5.9	48	9.3	238	37	2.9	2.1	15	-29.7
KPP7	78.2	0.24	4.5	2.5	0.55	0.23	0.90	4.4	9.2	0.47	75	169	0.44	133	22	6.0	69	16	268	56	5.1	2.4	15	-29.7
KP22	83.1	0.04	5.3	2.3	0.43	0.15	0.76	3.8	9.1	0.42	83	329	0.25	137	22	6.2	73	14	188	59	4.8	1.7	14	-29.8
KP21	85.8	0.56	7.3	1.8	0.25	0.86	0.76	3.4	7.1	0.47	68	354	0.19	125	18	6.9	86	21	224	89	9.0	2.6	12	-29.8
KP20	87.7	0.28	5.8	1.9	0.33	0.24	0.80	3.8	8.3	0.46	80	344	0.23	119	20	6.1	75	18	181	67	6.6	1.8	13	-29.8
KP19	90.7	0.36	6.9	3.1	0.45	0.34	0.76	4.6	8.1	0.57	83	101	0.82	141	20	6.9	96	19	176	87	7.3	1.8	14	-30.1
Unit 2																								
KP18	92.0	0.13	4.5	2.2	0.49	0.40	0.77	4.0	8.1	0.49	89	103	0.86	132	20	6.6	66	19	164	60	7.0	1.7	15	-30.1
KP17	95.0	0.46	6.8	2.2	0.32	0.24	0.49	2.5	5.2	0.48	49	265	0.18	133	20	6.8	54	14	124	78	7.9	2.0	8.0	-30.1
KP16	96.5	0.12	6.0	2.3	0.38	0.39	0.66	3.5	7.0	0.50	72	232	0.31	116	16	7.1	64	18	149	67	7.6	1.8	11	-30.2
KP15	98.1	0.15	5.7	2.0	0.35	0.37	0.62	3.1	6.7	0.46	67	251	0.27	127	17	7.3	60	17	159	66	7.6	2.0	11	-30.0
KP14	99.7	0.21	7.4	2.7	0.37	0.31	0.61	3.6	6.6	0.55	69	306	0.22	127	17	7.5	67	20	149	76	9.3	1.9	9.1	-29.6
KP13	101.2	0.43	11	2.3	0.22	0.28	0.68	3.3	6.8	0.49	65	321	0.20	113	17	6.5	53	17	121	58	7.4	1.5	5.1	-29.6
KP10	103.1	0.04	7.7	2.9	0.37	0.41	0.58	3.6	6.1	0.59	70	229	0.31	113	17	6.7	121	23	122	146	11	1.7	16	
KP12	105.1	0.01	7.7	3.5	0.46	0.25	0.58	3.9	6.2	0.63	62	102	0.61	98	15	6.4	108	22	128	129	11	1.7	14	-30.1
KP9	108.3	0.17	5.0	3.3	0.66	0.35	0.47	3.8	5.5	0.69	64	163	0.39	95	13	7.3	70	16	101	95	8.8	1.6	14	-29.8
KP8	110.1	0.01	7.1	3.6	0.51	0.41	0.58	4.2	6.3	0.66	80	97	0.82	105	16	6.6	84	20	119	98	10	1.6	12	-29.9
KP7	114.2	0.08	5.5	3.0	0.54	0.58	0.50	3.4	4.8	0.71	61	120	0.51	87	11	7.8	65	14	89	101	8.8	1.6	12	-30.0
KP6	118.2	0.49	9.3	4.2	0.45	1.5	0.78	4.6	4.8	1.0	64	140	0.46	105	12	8.9	125	30	113	192	18	2.0	14	-30.5
Unit 1																								
KP5	120.2	0.05	9.9	4.8	0.48	0.57	0.60	5.0	6.3	0.80	83	178	0.47	111	16	6.9	133	27	167	156	13	2.2	13	-30.5
KP4	123.0	0.51	12	6.0	0.49	0.71	0.75	6.2	6.7	0.92	79	60	1.3	129	17	7.7	59	26	139	65	12	1.8	4.8	-30.1
KP3	126.1	0.10	8.2	2.9	0.35	0.54	0.67	4.0	7.2	0.56	86	100	0.87	124	19	6.5	134	27	163	138	11	1.9	16	-30.4
KP2	128.6	0.07	13	3.2	0.24	0.38	0.62	4.2	6.8	0.62	68	91	0.75	114	16	7.1	115	26	125	125	11	1.5	8.7	-29.3
KP11	130.9	0.09	7.2	3.0	0.42	0.37	0.69	4.0	7.4	0.53	72	265	0.27	134	18	7.6	111	20	136	111	8.3	1.5	15	-30.5
KP1	135.3	0.25	14	2.3	0.16	0.29	0.69	3.5	7.3	0.48	78	147	0.53	172	20	8.8	152	38	548	153	15	6.3	11	-30.6

[a] TOC = total organic carbon

[b] TS = total sulfur

[c] EF = enrichment factor

Table 2

Table 2. Molybdenum and uranium isotope data for black shales of the Kettle Point Formation

Sample	Height (m)	Bulk $\delta^{98}Mo$[a] (‰)	Authigenic $\delta^{98}Mo$[a] (‰)	2SD Measured	2SD Reported[b]	n[c]	Bulk $\delta^{238}U$[d] (‰)	Authigenic $\delta^{238}U$[d] (‰)	2SD Measured	2SD Reported[e]	n[c]
Unit 4											
KPZ-1	28.0	0.82	0.82	0.05	0.11	3	0.54	0.60	0.07	0.08	3
KPZ-2	28.7	0.98	0.98	0.02	0.11	3	0.40	0.44	0.02	0.08	3
KPZ-2-rpt	28.7						0.39		0.01	0.08	2
KPZ-3	29.4	0.95	0.95	0.03	0.11	3	0.46	0.49	0.04	0.08	3
KPZ-4	30.6	0.85	0.88	0.03	0.11	3	0.40	0.44	0.01	0.08	3
KPZ-4-rpt	30.6	0.90		0.03	0.11	3					
KPZ-5	31.4	0.95	0.95	0.03	0.11	3	0.37	0.42	0.10	0.10	3
KPZ-6	32.9	0.76	0.77	0.00	0.11	3	0.18	0.28	0.03	0.08	3
KPZ-7	34.4	0.71	0.71	0.04	0.11	3	0.53	0.60	0.06	0.08	3
KPW6	36.0	0.68	0.68	0.04	0.11	3	0.44	0.52	0.06	0.08	3
KPW4	37.5	0.76	0.76	0.03	0.11	3	0.39	0.46	0.04	0.08	3
KPW5	39.5	0.78	0.78	0.05	0.11	3	0.41	0.44	0.03	0.08	3
KPW5-rpt	39.5						0.37		0.26	0.26	2
KPW3	41.2	0.69	0.69	0.05	0.11	3	0.42	0.51	0.08	0.08	3
KPW2	42.9	0.71	0.72	0.05	0.11	3	0.32	0.45	0.07	0.08	3
KPW1	44.1	0.68	0.69	0.03	0.11	3	0.30	0.49	0.04	0.08	3
KPR2	46.4	0.55	0.55	0.04	0.11	3	0.34	0.46	0.14	0.14	3
KPR6	48.6	0.88	0.88	0.03	0.11	3	0.35	0.41	0.07	0.08	3
KPR8	51.4	0.77	0.77	0.03	0.11	3	0.34	0.41	0.11	0.11	3
KPR11	53.5	0.79	0.79	0.11	0.11	3	0.32	0.37	0.10	0.10	3
KPR14	56.8	0.86	0.87	0.01	0.11	3	0.20	0.25	0.06	0.08	3
KPR17	58.8	1.29	1.32	0.02	0.11	3	0.12	0.15	0.02	0.08	3
KPR-17-rpt	58.8	1.33		0.04	0.11	3					
KPP11	61.6	1.26	1.27	0.01	0.11	3	0.11	0.16	0.11	0.11	3
KPP8	64.1	1.31	1.32	0.03	0.11	3					
Unit 3											
KPP4	73.9	1.06	1.07	0.07	0.11	3	0.20	0.26	0.04	0.08	3
KPP3	76.6	0.77	0.78	0.02	0.11	3	0.04	0.22	0.04	0.08	3
KP21	85.8	0.62	0.62	0.02	0.11	3					
KP20	87.7	1.10	1.11	0.06	0.11	3	0.03	0.09	0.06	0.08	3
Unit 2											
KP18	92.0	1.17	1.18	0.03	0.11	3	-0.06	-0.02	0.08	0.08	3
KP15	98.1	0.96	0.97	0.05	0.11	3	0.01	0.06	0.07	0.08	3
KP10	103.1	1.60	1.61	0.05	0.11	3	-0.06	-0.04	0.05	0.08	3
KP12	105.1	1.27	1.28	0.09	0.11	3	-0.07	-0.05	0.10	0.10	3
KP9	108.3	1.69	1.70	0.08	0.11	3	-0.12	-0.10	0.04	0.08	3
KP8	110.1	1.45	1.46	0.03	0.11	3	-0.14	-0.12	0.11	0.11	3
KP7	114.2	1.57	1.58	0.07	0.11	3	-0.15	-0.13	0.04	0.08	3
KP6	118.2	1.65	1.66	0.05	3.00		-0.24	-0.24	0.06	0.08	3
Unit 1											
KP5	120.2	1.27	1.28	0.02	0.11	3	-0.03	-0.01	0.03	0.08	2
KP4	123.0	2.02	2.05	0.08	0.11	3	-0.29	-0.29	0.07	0.08	3
KP3	126.1	1.22	1.23	0.05	0.11	3	-0.03	0.00	0.08	0.08	3
KP2	128.6	1.73	1.74	0.01	0.11	3	-0.11	-0.09	0.02	0.08	2
KP11	130.9	2.02	2.04	0.06	0.11	3	-0.11	-0.08	0.04	0.08	3
KP1	135.3	0.97	0.98	0.04	0.11	3	0.27	0.31	0.08	0.08	3
KP1-rpt	135.3	0.99		0.07	0.11	3	0.27		0.05	0.08	3

rpt denotes a replicate analysis

[a] Mo isotope data reported relative to NIST SRM 3134 = +0.25‰

[b] Reported uncertainty is the 2SD of replicate measurements or 0.11‰, whichever is greater

[c] Number of times MC-ICP-MS analysis was carried out on the sample solutions

[d] U isotope data reported relative to CRM 145 = 0‰

[e] Reported uncertainty is the 2SD of replicate measurements or 0.08‰, whichever is greater

Declaration of interests

☒ The authors declare that they have no known competing financial interests or personal relationships that could have appeared to influence the work reported in this paper.

☐The authors declare the following financial interests/personal relationships which may be considered as potential competing interests: